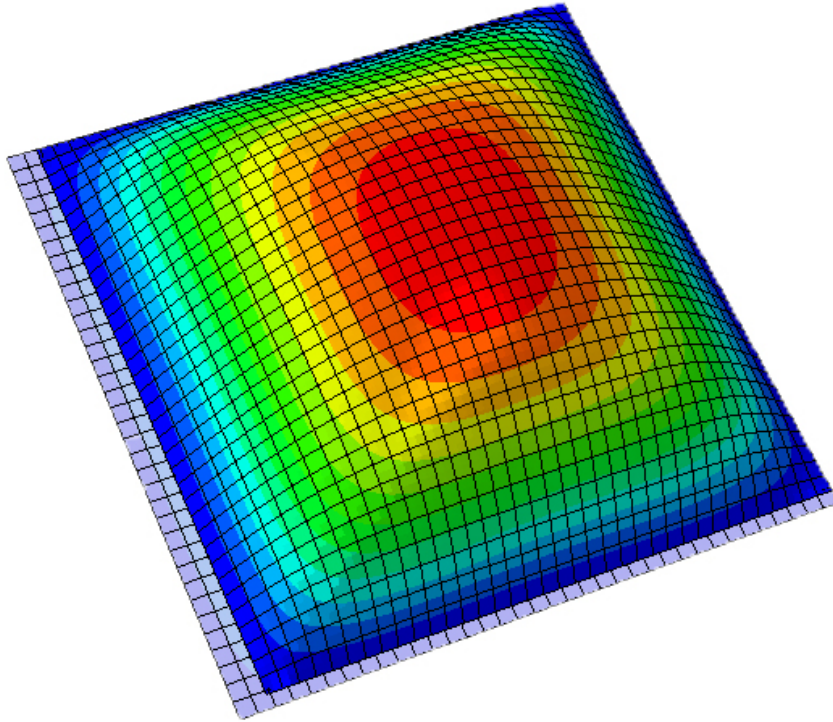


CHALMERS



Ultimate strength study of composite plates

Postbuckling analysis using semi-analytical methods

Master's Thesis in the International Master's Programme Naval Architecture and Ocean Engineering

ERIK BRAATEN AND JONAS BOSTRÖM

Department of Shipping and Marine Technology
Division of Marine Design, Research Group Marine Structures
CHALMERS UNIVERSITY OF TECHNOLOGY
Göteborg, Sweden 2013
Master's Thesis X-13/288

MASTER'S THESIS IN THE INTERNATIONAL MASTER'S PROGRAMME IN
NAVAL ARCHITECTURE AND OCEAN ENGINEERING

Ultimate strength study of composite plates

Postbuckling analysis using semi-analytical methods

ERIK BRAATEN AND JONAS BOSTRÖM

Department of Shipping and Marine Technology
Division of Marine Design
Research Group Marine Structures
CHALMERS UNIVERSITY OF TECHNOLOGY
Göteborg, Sweden 2013

Ultimate strength study of composite plates – Postbuckling analysis using semi-analytical methods

ERIK BRAATEN AND JONAS BOSTRÖM

© ERIK BRAATEN AND JONAS BOSTRÖM, 2013

Master's Thesis X-13/288

ISSN 1652-8557

Department of Shipping and Marine Technology

Division of Marine Design

Research Group Marine Structures

Chalmers University of Technology

SE-412 96 Göteborg

Sweden

Telephone: + 46 (0)31-772 1000

Cover:

Deflection of a square composite laminate, Abaqus CAE

Printed by Chalmers Reproservice

Göteborg, Sweden 2013

Ultimate strength study of composite plates – Postbuckling analysis using semi-analytical methods

Master's Thesis in the International Master's Programme in Naval Architecture and Ocean Engineering

ERIK BRAATEN AND JONAS BOSTRÖM

Department of Shipping and Marine Technology

Division of Marine Design, Research Group Marine Structures

Chalmers University of Technology

ABSTRACT

Highly energy efficient ships are valuable assets in the maritime transport industry; however, energy efficiency often comes at a higher price. In this work “energy efficient ships” are considered to be ships designed with lightweight structures, which lead to lower fuel-consumption or larger payload capacity. The material of the lightweight structures addressed in this thesis is fibre-reinforced plastic, a material known for its high strength to weight ratio. The material is also known to be expensive and traditional design principles with over-conservative estimates need to be reviewed in order to limit the costs.

The purpose of this thesis is to contribute to the development of methods for calculating the ultimate limit state (ULS) of fibre-reinforced plastic panels with less conservative estimates compared to traditional methods used in the industry. This contribution was achieved by extending the formulation of an existing computer software known as Panel Ultimate Limit State (PULS), which is used for estimating the ULS capacity for steel and aluminium panels, to include unstiffened single-skin composite panels. The ULS was defined as the ultimate load-carrying capacity. Two traditional lay-ups used in the maritime industry were analysed for different breadth/thickness-ratios under compressive load conditions. The results were compared with a finite element analysis and another semi-analytical model.

Through comparisons of the developed software against a finite element analysis, it is found that composite PULS provides reasonable conservative ULS results for plates with high breadth/thickness-ratios. Composite PULS has its limitations when it comes to estimating the ULS of plates with low breadth/thickness-ratios. It was experienced that the balance between accuracy and computational time is hard to establish.

Using composite PULS in order to estimate the ULS capacity is through this thesis shown to give a less conservative ULS compared to traditional design criteria. Composite PULS is based on Hashin-Rotem's failure criteria, and estimated the ULS to be 73-94% of the ULS calculated with a finite element analysis.

Key words: Buckling, composite panels, fibre-reinforced plastic, Hashin-Rotem's failure criteria, plates, semi-analytical method, strength, ultimate limit state.

Undersökning av brottgräns för plattor av komposit material - En utböningsanalys utförd med semi-analytiska metoder

Examensarbete inom Naval Architecture and Ocean Engineering

ERIK BRAATEN AND JONAS BOSTRÖM

Institutionen för sjöfart och marin teknik

Avdelningen för Marine Design, Forskargruppen Marine Structures

Chalmers tekniska högskola

SAMMANFATTNING

Energieffektiva fartyg är en värdefull tillgång inom transportindustrin, men hög energieffektivitet kommer med ett högt pris. Effektiva skepp beskrivs här kort som skepp tillverkade i lättviktsmaterial vilket möjliggör minskad bränsleförbrukning eller utökad lastnings förmåga. I denna studie behandlas lättviktsmaterialet fiberförstärkt plast, ett material som är känt för ett högt förhållande mellan styrka och vikt. Materialet betingar ett högt pris och förknippas med traditionella designprinciper med konservativa beräkningar som behöver ses över för att reducera onödiga kostnader.

Målet med denna studie var att bidra till utvecklingen av metoder som beräknar brottgränsen av fiberförstärkt plast på ett mindre konservativt sätt, jämfört med traditionella metoder. Detta har gjorts genom att utveckla en existerande programmjukvara, känd som ”Panel Ultimate Limit State” (PULS), vilket används för att uppskatta maximal lastbärnings förmåga för aluminium- och stålkonstruktioner, till att hantera fiberförstärkta plastpaneler. Två traditionella plastlaminat vanliga för den marina industrin, av olika tjocklekar och utsatta för kompressiva lastfall både axiellt och biaxiellt, har analyserats. Resultatet har jämförts med finita element analys och en alternativ semianalytisk modell.

Den utvecklade modellen, komposit PULS, har genom jämförelse med en finita element analys visats ge rimliga resultat för maximal lastbärnings förmåga för plattor med ett högt bredd/tjockleks förhållande. Vad beträffar plattor med lågt bredd/tjockleks förhållande så är möjligheterna att utföra en uppskattning av brottgränsen begränsade. Balansen mellan beräkningstid och resultatnoggrannhet visade sig vara svår att identifiera.

Det har i denna studie visats att komposit PULS ger en mindre konservativ bedömning av maximal lastbärningsförmåga än traditionella metoder. I komposit PULS har Hashin-Rotems brottkriterier använts och den uppskattade brottgränsen var på 73-94% av den maximala lastbärningsförmåga som uppnådes genom finita element modellen.

Nyckelord: Brottgräns, buckling, FRP-material, Hashin-Rotems brottkriterier, komposit paneler, plattor, semianalytiska metoder, styrka.

Contents

ABSTRACT	I
SAMMANFATTNING	II
CONTENTS	III
PREFACE	V
NOTATIONS	VI
1 INTRODUCTION AND MOTIVATION	1
1.1 Background	1
1.2 Objective	3
1.3 Methodology	4
1.4 Limitations and assumptions	5
1.5 Outline of thesis	6
2 MODEL INTRODUCTION	9
2.1 Panel Ultimate Limit State (PULS)	9
2.2 Complete ply degradation model (CPDM)	11
2.3 Progressive damage evolution	12
2.3.1 Composite failure modes	13
2.3.2 Progressive damage methods	16
2.3.3 Failure criteria	17
2.3.4 Tsai-Wu failure criterion	18
2.3.5 Hashin-Rotem and Hashin failure criteria	19
3 CPDM-COMPLETE PLY DEGRADATION MODEL	21
3.1 Convergence study of CPDM	21
3.2 Convergence study results	22
4 COMPOSITE PULS	25
4.1 Implementation of composite plates	25
4.1.1 Implementing of composite stiffness	25
4.1.2 Calculation of in-plane stresses and failure degradation	27
5 FINITE ELEMENT ANALYSIS	29
5.1 Abaqus model and material set-up	29
5.2 Boundary conditions and loadings	29
5.3 Damage evolution	30

5.4	Analysis procedure	31
5.5	Element type	31
5.6	Mesh convergence study	34
6	COMPARISON AND DISCUSSION OF POSTBUCKLING ANALYSES	37
6.1	Displacement description without failure	37
6.2	Uniaxial load cases	38
6.3	Biaxial load cases	45
6.4	Delamination	46
7	CONCLUSIONS	47
8	RECOMMENDATIONS FOR FUTURE WORK	49
9	REFERENCES	51
	APPENDIX A. CLASSICAL LAMINATED PLATE THEORY	A1
	APPENDIX B. FIRST-ORDER SHEAR DEFORMATION THEORY (FSDT)	B1
	APPENDIX C. ENERGY PRINCIPLES	C1
	Potential energy	C1
	Virtual work principles	C2
	The principle of minimum potential energy	C2
	APPENDIX D. RAYLEIGH-RITZ METHOD	D1
	APPENDIX E. COMPOSITE AND BUCKLING THEORY	E1
	APPENDIX F. COMPLETE PLY DEGRADATION MODEL (CPDM)	F1
	Displacement and load parameters	F1
	Failure initiation, material degradation and recalculation of material stiffness	F4
	APPENDIX G. EQUATIONS USED IN CALCULATION OF CRITICAL ENERGY RELEASE RATE	G1
	APPENDIX H. RESULTS MESH CONVERGENCE STUDY ABAQUS	H1
	APPENDIX I. RESULTS	I1

Preface

This thesis is a part of the requirements for the master's degree in Naval Architecture and Ocean Engineering at Chalmers University of Technology, Göteborg. It has been carried out from January to June 2013 at the Division of Marine Design, Department of Shipping and Marine Technology, Chalmers University of Technology in cooperation with Det Norske Veritas, Division of Maritime Advisory, in Høvik, Norway.

We would like to acknowledge and thank our examiner and supervisor, Professor Jonas Ringsberg at the Department of Shipping and Marine Technology, for his support and feedback throughout the period.

Further, we would like to acknowledge and thank our supervisor Dr. Philippe Noury along with Dr. Lars Brubak and Ole Jakob Hareide, M.Sc., at DNV for the opportunity of doing this thesis. Their supervision has been of great value.

We would also like to acknowledge and thank Professor Brian Hayman and PhD student Qiao Yie Yang at the University of Oslo for insight into their work and assistance along the way.

Our acknowledgments and thanks are due to co-supervisor PhD student Luis Sanchez at Chalmers University of Technology for his assistance in writing this report.

Finally, we would like to express our gratitude to everyone at the DNV-office who have helped and guided us during our work.

The figures presented in the report are used with permission from the publishers.

Göteborg, June, 2013

Jonas Boström and Erik Braaten

Notations

Roman upper case letters

A	Displacement amplitude	[mm]
[B]	Coupling stiffness matrix	[N]
[C]	Stiffness matrix for homogenous material	[MPa]
[C _d]	Degraded stiffness matrix	[MPa]
D	Damage parameter	[-]
[D]	Bending stiffness matrix	[Nmm]
E	Young's modulus	[MPa]
G	Shear modulus	[MPa]
L ^c	Length between nodes of an element	[mm]
N _{ref}	Reference load	[N/mm]
P ^N	Preload	[MPa]
Q ^N	Perturbation load	[MPa]
[Q]	Stiffness matrix	[MPa]
S	Shear strength	[MPa]
U ^b	Bending energy	[mJ]
V _f	Fiber volume fraction	[-]
X	Longitudinal strength	[MPa]
Y	Transverse strength	[MPa]
Z	Out of plane strength	[MPa]

Roman lower case letters

$d_{f,m,s}$	Damage factor; respectively fiber, matrix, shear	[-]
g	Shape function	[-]
m	Number of half sine waves along the x-direction	[-]
n	Number of half sine waves along the y-direction	[-]
w	Out-of-plane deflection	[mm]
x	Longitudinal coordinate	[mm]
y	Transverse coordinate	[mm]

Greek lower case letters

ε	Normal strain	[-]
ε^0	Mid-plane strain	[-]
ϕ	Rotation	[-]
γ	Shear strain	[-]
$\Delta\eta$	Increment parameter	[-]
λ	Eigen value	[-]
ν	Poisson's ratio	[-]
σ	Stress	[MPa]
τ	Shear stress	[MPa]

Subscripts

1	Longitudinal direction	[-]
2	Transverse direction	[-]
3	Out of plane direction	[-]
C	Compression	[-]
S	Symmetric	[-]
s	step	[-]
T	Tension	[-]

Abbreviations

ALS	Accidental limit state
CDM	Continuum damage mechanics
CLPT	Classical laminated plate theory
CPDM	Complete ply degradation model
CPT	Classical plate theory
DNV	Det Norske Veritas
DOF	Degrees of freedom
FE	Finite element
FEA	Finite element analysis
FFF	First fibre failure
FLS	Fatigue limit state
FPF	First ply failure
FRP	Fibre-reinforced plastic
FSDT	First-order shear deformation theory
GRT	Gross register tonnage
IMO	International Maritime Organisation
LPF	Load proportional factor
PULS	Panel ultimate limit state
SLS	Serviceability limit state
ULS	Ultimate limit state

1 Introduction and motivation

In this section, a brief introduction is presented, including the background, objective, methodology, limitations and outline of the thesis.

1.1 Background

Around 90% of the world's trade is today carried out at sea, and the trade volume is expected to increase in the forthcoming years, see IMO (2013). With this high share of the transport industry, it is important to realise our responsibility for reducing the harmful emissions caused by shipping, and making transport as energy efficient as possible. The introduction of alternative energy sources can reduce significantly the release of dangerous emission gases like SO_x , NO_x and CO_2 . Other aspects to consider are to reduce the resistance through the water by optimizing the hull shape or reduce the weight of the structure.

The structural weight can be reduced by using lightweight materials, such as aluminium and fibre-reinforced plastic (FRP). FRP structures are in general more expensive to fabricate than classical steel structures, but aspects like low maintenance, a long fatigue life and no corrosion contribute to a lower yearly cost compared to steel structures, see LIWEM (2012). The high strength to weight ratio of composites can be used for reducing the weight of the structure of a ship. By reducing the weight of the structure, there are possibilities of increasing the speed, reducing the fuel consumption and thereby the emissions, adding more cargo or increasing the stability by combining steel and composite structural designs, see LIWEM (2012) and RINA (2013).

There are many examples of where FRP has been applied and one such is a large fleet of small ferries. For small ferries the structural weight is a large proportion of the total load, and, subsequently, decreasing the structural load has large benefits on fuel consumption. An example on how the size of FRP-ferries has increased is U.T.O Krilo Carbo with its 546 gross register tonnage (GRT), see Brødrene AA (2013). Additional examples of FRP ships can be found in the Navy, where the Visby class corvette in the Royal Swedish Navy, see Kockums (2013), and the American destroyer, DDG-1000 Zumwalt class, planned to be delivered in 2014, see Naval-technology (2013) are such examples. Since the Navy does not have to comply with SOLAS rules, and as large budgets for rather complex structures are available, they have been able to exploit the benefits of FRP structures.

FRP have so far been of limited use in the maritime transport industry because of the high price associated with FRP constructions, but with increasing oil prices the profitability of utilising FRP is now highlighted. An example of a well-known operator in the maritime transport industry is Stena Teknik which came up with a concept design; Stena F-MAX, which saved 500 tonnes by introducing a FRP superstructure, see LIWEM (2012).

When designing ships, there are different limit state designs that describe different methods used in the design process.

- ALS, accidental limit state
- FLS, fatigue limit state
- SLS, serviceability limit state
- ULS, ultimate limit state

The ULS can be defined as the load condition where the structure fails due to reaching its maximum strength, potentially causing significant loss of lives or values, see Hollaway et al. (2001). It should be mentioned that ULS for FRP is defined in various ways in different available literature, where examples of such are; FPF, first buckling load, first fibre failure or maximum load-carrying capacity. The definition of ULS throughout the thesis was considered as the maximum load-carrying capacity of a plate. The SLS is defined as a condition where the structural response reaches a limiting value when performing normal use, while ALS is the condition where the safety of personnel, the cargo or the environment is affected due to accidents causing large structural damage. FLS is the condition where fatigue cracks due to long-term usage during operational conditions occur.

A common factor for these limit state designs is safety, where different situations a ship can experience throughout its lifetime are considered. For panels in ships subjected to hogging and sagging, the ULS in both compression and tensile load cases is of importance. The regulations for marine hull constructions using fibre composite materials developed by class are based on first ply failure (FPF) and buckling load, where matrix failure should be inhibited by the fibres in the composite, see DNV (2013 a). To ensure that the FPF or the first buckling load is not reached, a safety factor of 0.33-0.4, depending on the structure, is used for defining the limit load, see Figure 1.1. This consideration is conservative where the calculation time is low, but there is, however, often a significant amount of residual strength after the defined limit load. The deflection after the first buckling load, however, is non-linear and results in complex calculations.

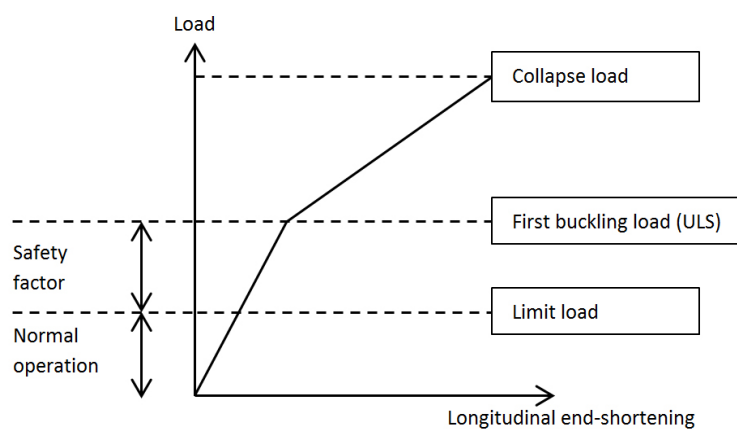


Figure 1.1 Principal load-displacement curve showing different load states for current traditional design scenarios.

By exploiting this residual strength in the postbuckling area the ULS and a less conservative limit load can be calculated, resulting in a more optimized structure. Figure 1.2 shows how the limit load is located closer to the first buckling load and FPF. The non-linearities that occur with large deflection and material degradation is often a complex task to describe, resulting in high computational costs.

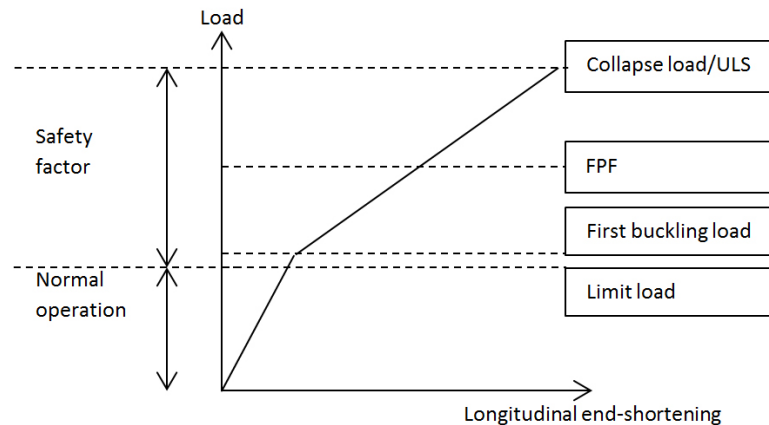


Figure 1.2 Principal load-displacement curve showing different load states for future design scenarios.

For thin-walled stiffened steel panels used in ship hull structures, there exists a semi-analytical computer software, PULS (Panel Ultimate Limit State) that increases the accuracy in ULS-calculations compared to traditional rule formulations, see DNV (2013 b). The ULS calculated by PULS accounts for residual strength in the postbuckling region. The computational cost is low and it allows for optimization in the design process.

The benefits of a similar tool for composite structures are obvious and will contribute to a less conservative ULS prediction than achieved with traditional designs. The purpose of this thesis has been to develop a computational tool that with tolerable accuracy can estimate the ULS capacity of FRP panels within reasonable time. An ongoing research project for developing a semi-analytical method for estimating the ULS-capacity of FRP panels is the Complete Ply Degradation Model (CPDM), see Yang (2013), and further testing of lay-ups typical for the maritime industry is of interest.

1.2 Objective

The use of fibre-reinforced plastic (FRP) panels in ships has large potentials regarding the contribution to a sustainable future. The high strength to weight ratio enables a lightweight structure design, although, on the other hand, the material cost is high. In order to reduce weight and cost it is important to reduce over-conservative designs. The objective of this thesis has been to make a fast and good assessment of the ULS of FRP-panels subjected to compressive loads. In more specific terms, the objective is expressed as:

- Extend PULS so that it can calculate the ULS of FRP-panels under compressive loads.

A more accurate assessment of the ULS would allow for improved utilization of FRP constructions. The improvement would result in a lower environmental impact, since unnecessary material can be avoided in both material fabrication and in structural design.

1.3 Methodology

In this section, a short description of the methodology used in order to achieve the objective is presented, see Figure 1.3 for a schematic overview.

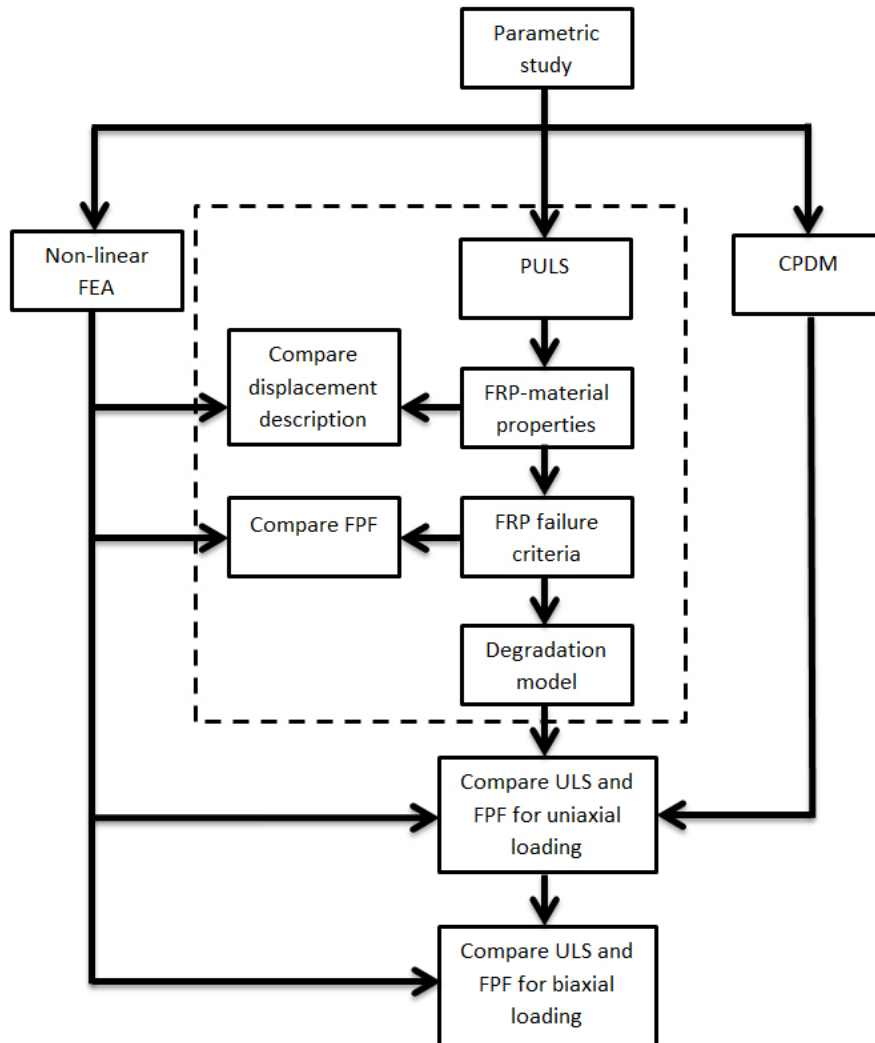


Figure 1.3 Flowchart of the methodology. The area surrounded by a dashed line shows the extension of PULS.

In order to extend PULS so that it could calculate the ULS of FRP-panels under compressive loads, the theory behind PULS was extended. The work was limited to a parametric study on square, single-skin, unstiffened panels of various b/t -ratios subjected to compressive loads, see Section 1.4 for a further description. The parts of PULS that were elaborated can be reduced to three areas; FRP material properties, FRP failure criteria, and a degradation model to evaluate the laminate strength after FPF.

The material properties were implemented using classical laminate plate theory (CLPT). The failure of the material was calculated through failure criteria developed by Hashin-Rothem, see Section 2.3.5. To estimate the ULS of the plate, a complete ply degradation model, see Section 2.3.2, was implemented utilizing the residual strength after FPF. The implementations were done using the programming language Fortran 95. Continuous validations of displacement descriptions, FPF loads and the implementation of a degradation model, see Figure 1.3, were performed with a non-linear FE-model as a reference.

Composite PULS was validated against both CPDM and a non-linear FEA. The non-linear FE-model was done in Abaqus Standard where two processes were performed. Firstly, a linear buckling analysis was performed in order to utilize the displacement description of the first buckling load as input for the later analysis. Secondly, the static Riks method was used in order to describe the load/displacement relation. The results gained from the FE-model were used for evaluating the ULS and FPF calculated for the parametric study with both composite PULS and CPDM for the uniaxial compressive load case. The biaxial compressive load case was only evaluated using composite PULS and Abaqus.

1.4 Limitations and assumptions

The study was carried out in cooperation with Det Norske Veritas (DNV) and Universitetet i Oslo, and limited to already existing models, namely PULS and CPDM, see Sections 2.1 and 2.2. The study is based on the background theory and assumptions of the already existing PULS. From the existing framework, the objective was to develop PULS to encompass composite material, and the limitations and assumptions regarding this further development are presented in this section.

It was unknown whether or not PULS would be extendable to include composite materials, and in order to keep the focus on the theoretical applicability simple plates were chosen. Simple plates mean that the geometry was limited to single-skin square-shaped panels without any stiffeners and with various thicknesses. The study cases consisted of investigating postbuckling failure for square panels with lengths of 500 mm. Different thicknesses were defined by a breadth to thickness ratio, b/t , which was given by 10, 15, 20, 30 and 50.

No plate is perfectly flat and therefore an initial imperfection of 0.1 % of the length was used, with the shape from the first buckling mode. There are many different composite material combinations to choose between, and in order to compare and develop PULS the study was limited to one material set-up. The material is FRP, made of a pre-preg E-glass fibre/epoxy, where the fibres are unidirectional. The material properties found through testing done by Hayman et al. (2011) were used. The material properties are found in Table 1.1, where the subscripts 1 and 2 are in the longitudinal and transverse directions, respectively, and T and C are tensile and compressive.

Table 1.1 Material Properties of the material used throughout the thesis.

Material properties		
$E_1 = 49627$ [MPa]	$G_{12} = G_{13} = G_{23} = 4800$ [MPa]	$\nu_{12} = 0.27$
$E_2 = 15430$ [MPa]	$V_f = 0.62$	
$X_T = 968$ [MPa]	$Y_T = 24$ [MPa]	$S = 65$ [MPa]
$X_C = 915$ [MPa]	$Y_C = 118$ [MPa]	

The lay-up configurations chosen, see below, are commonly used in the shipping industry and give additional test results for the CPDM.

- Lay-up A, a quadriaxial lay-up: $[0_3 / + 45 / 90 / - 45]_{2s}$
- Lay-up B, a triaxial lay-up: $[- 45 / + 45 / 0]_{4s}$

The loads applied were restricted to uniaxial and biaxial compression for simply supported boundary conditions, since these boundary conditions cause the lowest ultimate load, see Misirlis (2012).

1.5 Outline of thesis

The thesis is divided into eight sections, where Section 1 describes the introduction and motivation behind the work. After this section the reader should have a clear view of the objective, how the objective was solved and which limitations and assumptions that were made in order to fulfil the work.

In Section 2, the theories behind the models are presented in short terms. An introduction to failure theory, failure criteria and progressive failure is given in order to give an understanding of the later sections.

The work done by the authors regarding the CPDM is explained in Section 3.

In Section 4, the development of PULS to include composite materials is explained. The implementation of stiffness matrices, decisions of progressive failure and in-plane stress calculations are described. Further, the limitations regarding these choices are motivated.

Section 5 introduces the FE-model in terms of analysis procedure and the damage evolution model. The choice of element type as well as mesh size is motivated and described.

Results are compared and discussed in order to form an understanding of the performance of the models in Section 6.

In Sections 7 and 8 the conclusions of the thesis and future work, respectively, are presented.

The Appendix section contains further descriptions of the theories applied in the different models in form of mathematical expressions. The rest of the results that are not presented in Section 6 are found in the Appendix.

2 Model introduction

In this section an introduction to the Complete Ply Degradation Model (CPDM), the Panel Ultimate Limit State (PULS) and failure theory are presented. Further explanations of the theories mentioned in the text are found in the appendices.

2.1 Panel Ultimate Limit State (PULS)

PULS stands for Panel Ultimate Limit State. It is a semi-analytical software for an estimation of ULS through the non-linear buckling behaviour of steel panels developed by DNV (2013 b). PULS estimates the ULS capacity of plates that are unstiffened, regularly stiffened, arbitrarily stiffened, open corrugated and subjected to uniaxial and biaxial compressive, shear and tension loads. The software is used as a tool combined with linear FEA from where loads are extracted in order to make a more thorough assessment of the design. PULS can, for example, be used in the estimation of a ULS capacity of structures that through years of service have been exposed to corrosion.

The software is based on the large deflection plate theory developed by von Karman and Marguerre, where Marguerre extended the non-linear theory developed by von Karman to account for the initial imperfections in the plate, see Byklum (2002). The non-linear terms introduced by von Karman are necessary in order to achieve a better approximation of the membrane strains when the deflection is relatively large compared to the thickness, see Turvey et al. (1995). The membrane strains are one part of the total strains which, in PULS, are expressed by using Kirchhoff's assumptions:

- Straight lines perpendicular to the mid-plane (transverse normals) remain straight as the plane deforms into a surface, see Figure 2.1.
- Transverse normals do not experience elongation.
- The transverse normals rotate in such a way that they remain perpendicular to the mid-surface after deformation.

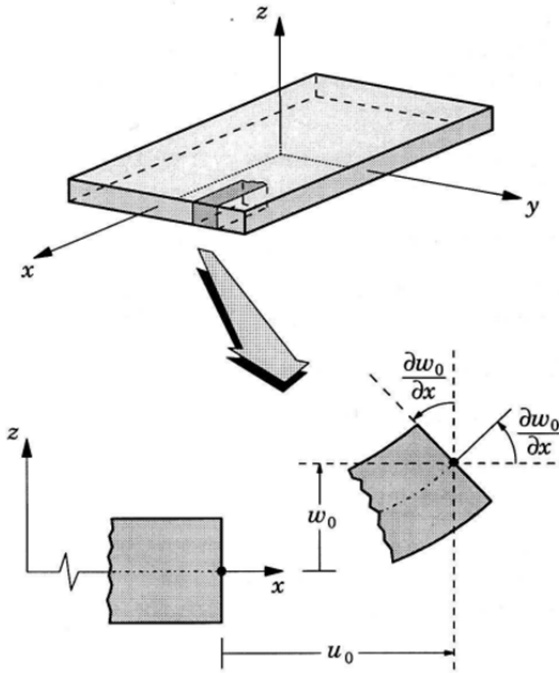


Figure 2.1 Undeformed and deformed plate geometry when Kirchhoff's assumptions hold, see Reddy (2004).

These assumptions are valid for plates with a side-to-thickness ratio greater than 30, see Reddy (2007), for thicker plates first-order or higher order shear deformation theories could be required.

In order to develop the non-linear elastic equilibrium equations due to the large deformation theory, energy methods like the virtual work principle and the principle of minimum potential energy are used, explained in detail by Byklum (2002). For both principles, see Appendix C, the work done by external and internal forces are required and these are described by the mid-plane deflection, w . To describe the deflection in connection with the principle of minimum potential energy, the Rayleigh-Ritz method has shown to be convenient, see Byklum (2002). The Rayleigh-Ritz method, see Appendix D, reduces the problem that describes the deflection, and to find the amplitudes of the shape functions, see Equation (2.1). The number of terms required is dependent on how well the chosen shape functions agree with the actual deflection.

$$w(x, y) = \sum_m \sum_n A_{mn} g_m(x) g_n(y) \text{ [mm]} \quad (2.1)$$

where g_m and g_n are shape functions and A_{mn} are displacement amplitudes. Using the deflection keeps the number of terms low, since only one dimension is regarded. However, the choice of shape functions is critical when only one parameter is regarded, see Chia (1980). Instead of expressing the energy by the deflection, an alternative is to express it with displacements in the x , y and z directions. To express the energy by displacements in all directions would include more terms, which results in higher computational costs.

Byklum (2002) shows that the solution to the energy problem of a plate subjected to large deflection is of the fourth order in the deflection. This is reduced to the third order in the displacement amplitudes by implementing Rayleigh-Ritz and potential minimum energy. The non-linear system is made stepwise linearly by using a perturbation theory which calculates the next step by using the tangent in the previous step, explained in detail by Steen (1998).

The ULS-capacity for the steel plate is defined when the von Mises yield criterion is violated somewhere at one of the supported edges. The reason for only investigating the edges is that the stress can be redistributed to the edges until the yield criterion at the edges is reached. By investigating the edges only, the computational effort is reduced.

2.2 Complete ply degradation model (CPDM)

This method was established by Yang et al. (2012) as a semi-analytical model for estimating ULS capacity of unstiffened single-skin composite panels, and further developed in 2013, see Yang (2013), to account for the large deflection theory. A short introduction of the model is presented in the following text and is explained schematically in Figure 2.2. Each step of the method is explained further in Appendix F, and if a more detailed description is required, see Yang (2013).

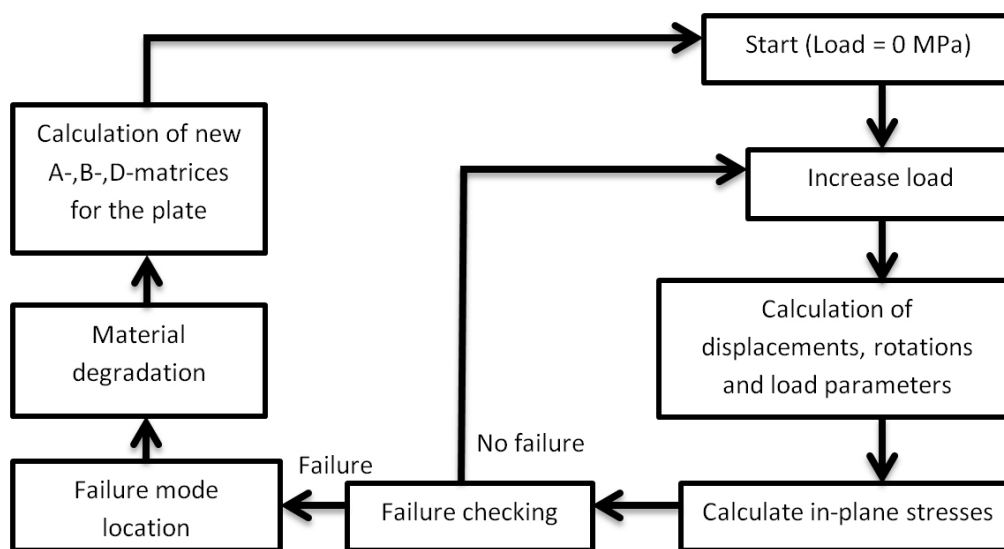


Figure 2.2 Schematic view of CPDM.

CPDM is based on the Rayleigh-Ritz method and is a general model in the sense that it accounts for unsymmetrical lay-ups and is based on FSDT, see Appendix B. FSDT is an extension of Kirchhoff's assumptions where the transverse normals must still be straight but not necessarily perpendicular to the mid-surface, see Figure 2.3. The consequence is that the cross section rotates with respect to the mid-plane, and these rotations must be accounted for.

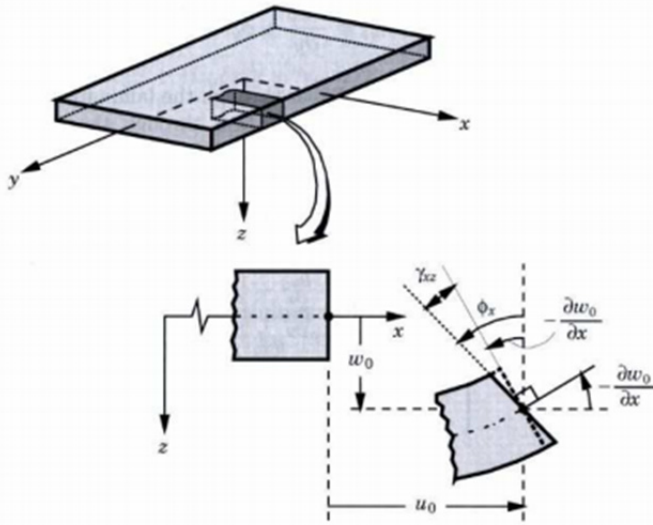


Figure 2.3 Undeformed and deformed geometries of a plate under the assumptions of the first-order plate theory, Reddy (2004).

CPDM expresses the displacements and cross sectional rotations via a Fourier series for each parameter, see Equations (F.1) to (F.5) in Appendix F. These parameters are implemented in Rayleigh-Ritz and a similar procedure as for PULS is performed. The displacements and rotations are used for expressing the energy problem and the last unknowns are solved with the perturbation method.

Accounting for unsymmetrical lay-ups means that there is a coupling between the in-plane forces and moments, i.e. the coupling matrix $\mathbf{B} \neq 0$, which does not allow for the large matrix in Equation (A.13) to be divided into smaller sub-matrices. The reason for including the coupling matrix, even though many laminates are symmetric, is that when the material is degraded the lay-up becomes unsymmetrical and hence the symmetry condition is no longer fulfilled.

As a plate is subjected to an increasing load, the matrix and/or fibres of the composite will eventually fail in different failure modes, see Section 2.3.1. When failure occurs, the matrix and/or fibres are damaged meaning that the stiffness of the material is reduced resulting in a weaker structure. There are several ways of accounting for the strength reduction, where the CPDM reduces the stiffness contribution from the failed part (matrix and/or fibres) for the complete ply. The material is degraded until the maximum load is achieved and this load then defines the ULS.

In the study performed by Yang (2013), two lay-ups were used, one triaxial $[-45/+45/0_4/+45/-45/0_4/-45/+45/0_3]_s$ and one quadriaxial $[0/+45/90/-45]_{x,s}$. The ULS results calculated with CPDM varied from 67% to 87% compared to the ULS achieved using the FEA approach performed by Hayman et al. (2011).

2.3 Progressive damage evolution

When describing the process from first ply failure (FPF) to the ULS for a composite laminate, failure criteria and progressive damage evolution should be mentioned. In

this section, different failure modes as well as failure criteria are presented in order to describe progressive damage models.

2.3.1 Composite failure modes

To describe failure of an FRP material, different failure modes should be considered. The failure can be divided into internal material failure, also known as microscopic failure, and macroscopic failure. Most often an internal failure is present before any macro failure is visible. According to Agarwal et al. (2006), the most typical ways of describing internal material failure are:

1. Breaking of the fibres
2. Micro-cracking in the matrix
3. Separation of fibres from the matrix (debonding)
4. Separation between laminas, also known as delamination

The different failure modes are closely connected to the loading conditions, material properties and lamina stacking. In the following text different failure modes in association with typical loading conditions are described.

For longitudinal tensile loads, breakage of the fibres often occurs at the weakest point in the cross section. There are three typical failure modes, described as; brittle failure, brittle failure with fibre pull-out, brittle failure with fibre pull-out and matrix shear failure or debonding.

Brittle failure is most common in composites with a low fibre volume fraction. In composites with a fibre volume fraction between 40% and 65% brittle failure with fibre pull-outs caused by stress concentrations at the fibre ends is the most common. Brittle failure with pull-outs and additional interface-matrix shear failure or debonding is typical for composites with a fibre volume fraction larger than 65%, see Agarwal et al. (2006), see Figure 2.4 for failure illustrations.

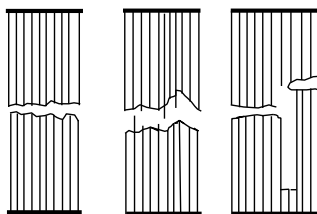


Figure 2.4 Failure modes for longitudinal tensile loads, from left; brittle failure, brittle failure with fibre pull-out, brittle failure with debonding/shear failure.

During longitudinal compressive loads, the most common internal failure modes, according to Agarwal et al. (2006), are transverse tensile failure, fibre micro-buckling and shear failure. Transverse tensile failure means that the composite is split along the fibre direction. This splitting is caused by transverse strains from the Poisson's ratio-effect that are larger than the ultimate transverse strain of the composite. Fibre micro-

buckling can be described in two ways, see Figure 2.5. The buckling with parallel fibres is the most common mode in composites with a fibre volume fraction above 40%. Fibre buckling is initiated after matrix yielding, micro-cracking or debonding. The third typical failure mode is shear failure, see Figure 2.6.

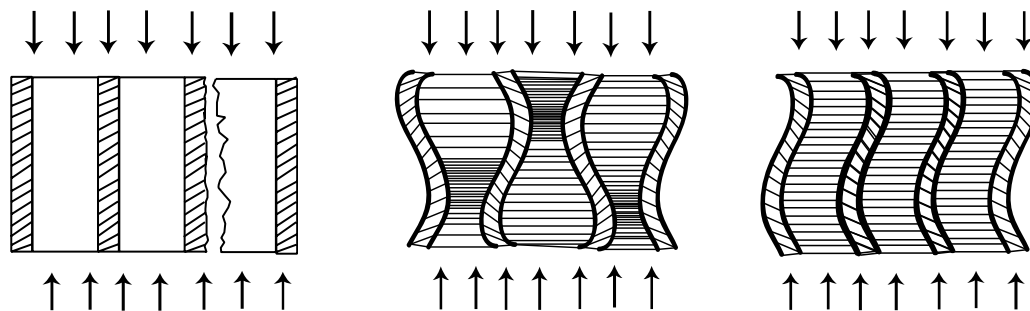


Figure 2.5 Failure modes for longitudinal compressive loads; (left) longitudinal compression loads, (middle) transverse tensile failure and (right) micro-buckling.

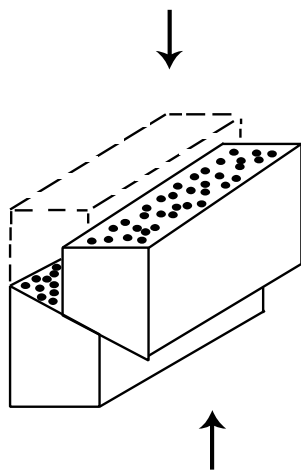


Figure 2.6 Shear failure for longitudinal compressive loading.

When the laminate is subjected to transverse tensile loading, common failure modes are: matrix tensile failure, debonding and fibre splitting. Loads transverse to the fibre direction cause stress concentrations in the matrix and in the interface between matrix and fibre, which lead to tensile matrix failure, see Figure 2.7. In the case of fibres with low transverse strength, a splitting of the fibre may occur.

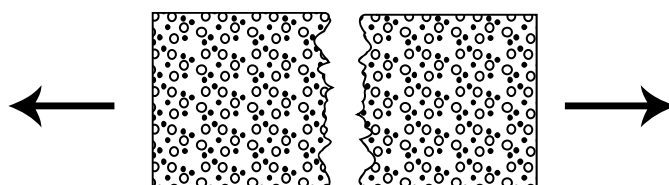


Figure 2.7 Matrix tensile failure.

During transverse compressive loading, typical failure modes are matrix shear failure and matrix shear failure with debonding/fibre crushing. The fracture splits the ply in an angle that depends on the interaction between the transverse and in-plane shear stresses, see Figure 2.8.

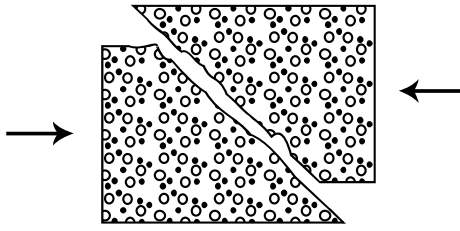


Figure 2.8 Matrix shear failure during transverse compressive loading.

For in-plane shear loads three failure modes are considered likely to happen; matrix shear failure, debonding with and without matrix shear failure, see Figure 2.9.

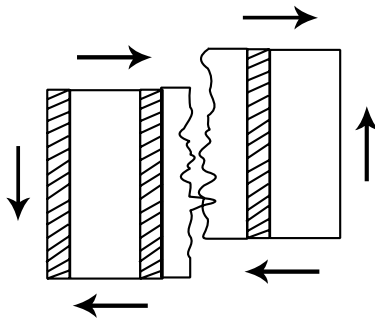


Figure 2.9 Matrix shear failure during in-plane shear loads.

Delamination is considered as an important failure mode, since it separates plies from each other preventing the load-distribution between the plies, see Figure 2.10. Instead, the laminate is reduced to individual plies that reduce the global strength significantly. Kageyama et al. (1991) and Turvey et al. (1995) claim that the most common cause of delamination is impact by foreign objects after the laminate has been loaded (in service). Delamination is also known as a result of several micro-cracks in the matrix, fatigue, inadequate bonding between layers or overload. The loading condition that is most associated with delamination is inter-laminar shear contribution, see Kageyama et al. (1991). An equation that expresses various load contributions is a stress-based failure criterion proposed by Ye (1988). The Ye criterion consists only of out-of-plane stress contributions, see Equation (2.2). If the normal stress is not tensile, the expression is reduced to shear contributions only.

$$\left(\frac{\sigma_{33}}{Z_T}\right)^2 + \left(\frac{\sigma_{13}}{S_{13}}\right)^2 + \left(\frac{\sigma_{23}}{S_{23}}\right)^2 \geq 1 \quad (2.2)$$

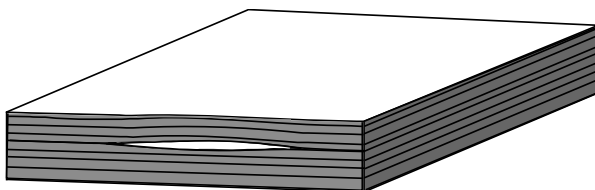


Figure 2.10 Delamination indicated by separated plies.

2.3.2 Progressive damage methods

The term damage evolution can be defined as a non-linear deformation process including three phases; nucleation of micro-defects, growth of the micro-crack and the development into a macro-defect, see Krajcinovic (1989). From the point where failure occurs from the micro-defects is a fact, the remaining fracture process should be described until final failure. Three methods that are, according to Hu et al. (2010), well known for describing the failure of composite laminates: the stress method, the fracture mechanics method and the continuum damage mechanics method.

The stress method determines the stresses either in each ply and/or between the plies in a laminate. Through the use of energy-principles and equilibrium equations in combinations with stress-strain relations and material constants, stresses can be determined. Cui et al. (2009) used this method for predicting damage initiation and residual tensile strength during internal failure in a laminate. The method, in combination with failure criteria, can only predict failure initiation and in order to describe further failure, either fracture mechanics or continuum damage mechanics (CDM) should be applied.

The fracture mechanics method can be described by the strain-energy release rate, stress-intensity factor and the J-integral, see Agarwal et al. (2006). During loading, the material absorbs energy by material deformation and the creation of new surfaces. The energy release rate is based on a criterion stating that the free energy of the cracked form and applied forces is not to increase as the crack is developing. The stress-intensity factor is the stress distribution around the crack tip. By assuming the composite material to be homogeneously anisotropic, expressions for the stress distributions around the tip can be determined. The J-integral is an energy line surrounding the crack-tip that is related to the plastic stress and strain singularities. Fracture mechanics is based on an initial crack or defects, and predictions of the crack growth and its path are often found complex to predict, see Hu et al. (2010).

The continuum damage mechanics model determines, through the use of internal state variables, the changes in the shape and form of the laminate, see Hu et al. (2010). In the term of damage evolution, these variables are often known as damage factors, which are used to reduce the material properties, see Equation (2.3) and Abaqus (2012), in order to describe a stress-displacement relation, see Figure 2.11.

$$[C_d] = \frac{1}{D} \begin{bmatrix} E_1(1-d_f) & E_1\nu_{21}(1-d_f)(1-d_m) & 0 \\ E_2\nu_{12}(1-d_f)(1-d_m) & E_2(1-d_m) & 0 \\ 0 & 0 & GD(1-d_s) \end{bmatrix} \text{ [MPa]} \quad (2.3)$$

where Poisson's ratio is represented by the D -term:

$$D = 1 - (1-d_f)(1-d_m)\nu_{12}\nu_{21} \quad (2.4)$$

Examples of damage factors can be terms that seek to reduce the material properties defining the fibre, matrix and/or the shear strength, see the d -terms in Equation (2.4). The development of these variables describes the evolution of the damage, and they can be classified as constants for sudden degradations and functions with different numbers of variables for gradual degradations, see Garnich et al. (2009). Figure 2.11

describes a stress-displacement relation where the terms, σ and δ^f , are made equivalent in order to avoid a strong mesh dependency. The relation is linear elastic until failure occurs in point A, and the further description of the stress-displacement relation is determined either by a sudden degradation or a gradual degradation. A sudden degradation would follow the vertical line from point A to D, which results in no residual strength. A gradual degradation would follow the line A-B-C if it is linear, where the stress-displacement relation is linear elastic between O and B as the strength is gradually reduced. The gradual degradation decreases the stiffness on the ply-level, while sudden degradation often is connected with complete ply degradation or degradation of elements on the ply-level.

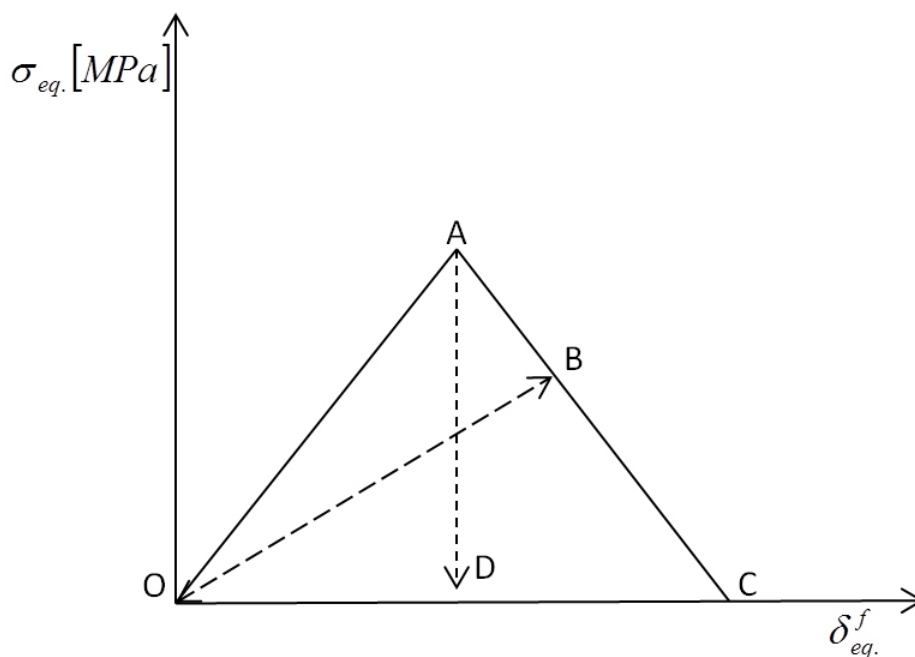


Figure 2.11 Example of a degradation scheme; sudden degradation between points A and D, and gradual degradation between A, B and C.

2.3.3 Failure criteria

Several failure criteria exist in order to estimate at which load failure occurs in a material. Failure criteria can be divided into two groups, stress-based criteria and fracture mechanics-based criteria. The fracture mechanics criteria are based on methods described in Section 2.3.2, while the stress-based criteria can be divided into mode-dependent and mode-independent, see Garnich et al. (2009). Traditional criterion like Tsai-Wu and Hashin, where Tsai-Wu is mode-independent and Hashin is mode-dependent, are well known through the last 30-40 years. They are easy to use, and their results have shown to give good agreement with experimental results. Hinton et al. (2002) have tested several failure criteria in order to highlight strengths and weaknesses of the methods. For traditional failure-mode independent criteria (Examples are Tsai-Hill, Tsai-Wu, Hoffman), Tsai-Wu proved to be the most reliable one compared to experiments. For mode-dependent criteria (Examples are Hashin-Rotem, Puck, Maximum stress/strain), the Puck criterion gave good results. The Puck criteria focus in the same way as Hashin on failure modes by distinguishing between fibre failure and matrix-failure. However, Puck failure criteria have shown to be less

accurate for structures with large displacements, see Hinton et al. (2002). Due to the similarities between Hashin and Puck, and the complexity in predicting the action-plane angle used in Puck's criteria, see Deuschle (2013), only the Hashin failure criteria will be introduced in this section. The criteria that are further presented, in Section 2.3.4-5 are the Tsai-Wu, Hashin-Rotem and Hashin failure criteria.

2.3.4 Tsai-Wu failure criterion

The failure criterion suggested by Tsai and Wu is a general stress expression based on interaction between stress components, see Equation (2.5):

$$F_i \sigma_i + F_{ij} \sigma_i \sigma_j = 1 \quad (2.5)$$

where $i, j = 1, 2, \dots, 6$

The F-terms are functions of uniaxial and biaxial strengths found through experiments, where most of the F-terms are given by simple expressions, Equation (2.6), see Tsai et al. (1971):

$$\begin{aligned} F_1 &= \frac{1}{X_T} - \frac{1}{X_C} \\ F_{11} &= \frac{1}{X_T \times X_C} \\ F_2 &= \frac{1}{Y_T} - \frac{1}{Y_C} \\ F_{22} &= \frac{1}{Y_T \times Y_C} \end{aligned} \quad (2.6)$$

The subscripts T and C, respectively, mean tension and compression. If Equation (2.5) is written in its full length with all the stress interactions and interaction terms, it would be difficult to operate. In total, there are 21 F_{ij} -terms and 6 F_i -terms, but simplifications can be done with regard to symmetry, transverse isotropy, and in-plane stress. Expressions similar to Equation (2.6) exist for most of the interaction terms, but F_{12} , F_{23} and F_{13} are not easily expressed. These terms should be found through biaxial failure testing, see Tsai et al. (1971). The interaction terms similar to Equation (2.6) are based on both compressive and tensile strengths, which, according to Hashin (1980), is unreasonable since a compressive stress-failure situation should be calculated with compressive strengths and not tensile strengths.

Although the Tsai-Wu criterion has shown to give a good fit with test results, there are disagreements concerning failure in different modes. It has been shown how different loading conditions result in different failure modes, see Hashin (1980). In order to identify failure modes, failure indices identifying the primary load direction relative to failure have to be defined. These failure indices have shown to be unpredictable when different indices are close in magnitude, see Garnich et al. (2009).

2.3.5 Hashin-Rotem and Hashin failure criteria

Hashin and Rotem suggested failure criteria based on experimentally observed failures for different loading conditions and different failure modes. The argumentation for the different modes is that in a plane where the failure occurs, the failure is caused by normal and shear stresses in that plane, see Hashin et al. (1973). In total, four failure criteria modes, both with Hashin-Rotem and the criteria later developed by Hashin, see Hashin (1980), will be presented. The difference between the two sets of failure criteria is that Hashin includes out-of-plane normal and shear stress contributions, while Hashin-Rotem are more simplified expressions with only in-plane stress contributions.

Tensile fibre mode:

Hashin-Rotem express the tensile fibre strength in the longitudinal direction by the maximum stress criteria, see Equation (2.7). For the criterion later developed by Hashin, see Equation (2.8), where the contributions of both in-plane and out-of-plane shear stresses are presented.

Hashin-Rotem:

$$\left(\frac{\sigma_{11}}{X_T}\right)^2 = 1 \quad (2.7)$$

Hashin:

$$\left(\frac{\sigma_{11}}{X_T}\right)^2 + \left(\frac{\sigma_{12}^2 + \sigma_{13}^2}{S_{12}S_{13}}\right)^2 = 1 \quad (2.8)$$

Compressive fibre mode:

In this mode, only the normal compressive stress, σ_{11} , is included, see Equation (2.9). The effect of axial shear stresses on the compressive strength was unknown at the time of the publication of the criterion, and therefore it is not included. Later tests that were done on the subject, see Michaeli et al. (2008), show that the fibre tensile strength is not significantly affected by shear stresses. For the compressive strength, only tests including small magnitudes of shear stress were done, and these tests show that shear stress has a small effect on the compressive strength, see Michaeli et al. (2008). For this statement to be valid, similar tests for larger shear stress magnitudes should be included. Based on the existing test-results, see Michaeli et al. (2008), the Hashin-Rotem tensile/compressive fibre failure criteria are found to be good approximations.

Hashin-Rotem and Hashin:

$$\left(\frac{\sigma_{11}}{X_C}\right)^2 = 1 \quad (2.9)$$

Tensile matrix mode:

The matrix failure modes are considered to be more complex compared to the fibre modes. This is due to the significant contribution of shear stresses, which makes it difficult to predict the failure plane.

Compared to the fibre failure mode, an in-plane shear contribution is considered as being of importance for the matrix failure in Hashin-Rotem for both tensile and compressive failure, see Equations (2.10) and (2.12). In Hashin, see Equations (2.11) and (2.13), stress contributions in terms of out-of-plane normal and shear stresses were added.

Hashin-Rotem:

$$\left(\frac{\sigma_{22}}{Y_T}\right)^2 + \left(\frac{\sigma_{12}}{S_{12}}\right)^2 = 1 \quad (2.10)$$

Hashin:

$$\left(\frac{\sigma_{22}\sigma_{33}}{Y_T Z_T}\right)^2 + \frac{\sigma_{23}^2 - \sigma_{22}\sigma_{33}}{S_{23}^2} + \frac{\sigma_{12}^2 + \sigma_{13}^2}{S_{12}S_{13}} = 1 \quad (2.11)$$

Compressive matrix mode:

Hashin-Rotem:

$$\left(\frac{\sigma_{22}}{Y_C}\right)^2 + \left(\frac{\sigma_{12}}{S_{12}}\right)^2 = 1 \quad (2.12)$$

Hashin:

$$\begin{aligned} & \left(\frac{Y_C Z_C}{2S_{23}^2} - 1\right) \left(\frac{\sigma_{22}}{Y_C} + \frac{\sigma_{33}}{Z_C}\right) + \left(\frac{\sigma_{22} + \sigma_{33}}{2S_{23}}\right)^2 \\ & + \frac{\sigma_{23}^2 - \sigma_{22}\sigma_{33}}{S_{23}^2} + \frac{\sigma_{12}^2 + \sigma_{13}^2}{S_{12}S_{13}} = 1 \end{aligned} \quad (2.13)$$

For thin shells, a general consideration is that the magnitude of the out-of-plane shear stress is considered small and of less importance, see Reddy (2004). Based on this consideration, it is assumed that Hashin's failure criteria will have a bigger contribution for thicker plates. Due to the tests done by Michaeli et al. (2008) it is believed that by applying Hashin instead of Hashin-Rotem, the difference will be most visible in the FPF region, while the ULS dominated by fibre-failure will remain the same.

3 CPDM-Complete Ply Degradation Model

In this section the extended validation of CPDM, which includes two more lay-up configurations, see Section 1.4, that are likely to be used in ship panels is presented. In order to get reliable results a convergence study for the new lay-ups was performed and can be reviewed in Section 3.1, and the results of the convergence study are presented in Section 3.2. The results of the extended validation are presented in Sections 6.1 and 6.2 where they are compared and discussed with composite PULS and Abaqus. CPDM and previous work done with CPDM are summarized in Section 2.2.

3.1 Convergence study of CPDM

For a given lay-up with all material data available, there are still parameters in CPDM that need to be defined in order to achieve reliable ULS results. Because the computation expense is limited and preferably small, the number of terms expressing the displacements/rotations, see Equations (F.1) to (F.5) in Appendix F, and the amount of increments in the incremental procedure need to be restricted. The convergence study along with the assumptions made are explained and motivated. The purpose of the scheme is to ensure convergence while minimizing the calculation time for a complete calculation.

Since the behaviour of the laminates is highly dependent on the lay-up configuration, a convergence study was performed using the new lay-ups. To limit the convergence study, all Fourier's series were assumed to need the same amount of terms, meaning that the displacement/rotation that converged the slowest determined the number of terms. The amount of increments is dependent on two parameters: the increment parameter $\Delta\eta$ and the reference load which $\Delta\eta$ relates to. In order to achieve approximately the same $\Delta\eta$ for different b/t -ratios the reference load was set to be half the buckling load for plates with a high b/t -ratio and smaller for plates with a low b/t -ratio. The reason for smaller reference loads for plates with a low b/t -ratio is that the compression strength of the material is the limiting factor rather than the buckling load, which is the limiting factor for plates with a high b/t -ratio.

The convergence for $\Delta\eta$ and the number of terms was investigated by the trial and error principle, including as few increments as possible without compromising the result. With the reference load set, the increment size needed was investigated. The load for the FPF was calculated for a rather large increment size, and this was then halved and the FPF was recalculated. The procedure was repeated until at least 150 increments and the recalculated load was no more than 1% of the previously calculated load, see Figure 3.1. The increment size affects the ability to describe the non-linear effects caused by the out-of-plan displacement. This effect means that if the effects from non-linearities are small, fewer increments are needed to trace the load-displacement curve. In order to limit the calculation time, five numbers of terms were used. The convergence of the increment load was checked for a larger number of terms for layups with the lowest b/t -ratio, since these were affected most by the number of terms.

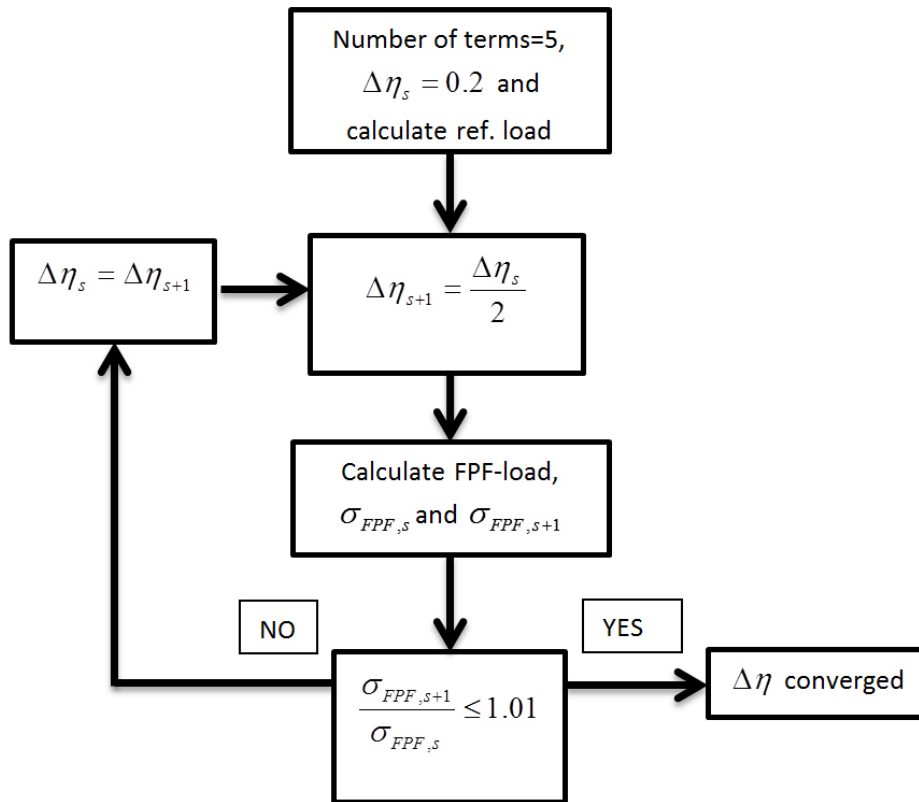


Figure 3.1 Flowchart of the convergence study of the increment parameter $\Delta\eta$.

3.2 Convergence study results

In this section the results from the convergence study are presented.

The results for Layup A, with $b/t=50$, are presented in Table 3.1

Table 3.1 Results from convergence of the increment size for lay-up A, $[0_3/+45/90/-45]_{2s}$ with $b/t=50$, reference load=162 N/mm and number of terms=5.

σ_{FPF} [MPa]	$\Delta\eta$	Number of increments	Buckling load [N/mm]
39.0	0.2	14	162
38.2	0.1	27	162
37.0	0.05	50	162
36.3	0.025	97	162
35.9	0.0125	190	162
35.7	0.0063	377	162

The number of terms for each lay-up was evaluated with the converged increment size and for first fibre failure (FFF). In order to decrease calculation time, total matrix failure was assumed meaning that degradation for matrix failure in all plies was adopted. Calculations of FFF for an increasing number of terms were made until convergence was achieved. However, if convergence was found at a larger number of terms than five, the convergence for the increment size was checked for the higher number of terms as well.

For plates with a low b/t -ratio, five numbers of terms were shown to be sufficient, while for plates with a high b/t -ratio the number of terms were needed in order to describe the displacements. Since large out-of-plane displacement was expected for plates with a high b/t -ratio, the demand for more terms was expected. In other words, the displacements are harder to describe when the out-of-plane displacements are large. Table 3.2 shows the convergence results for Lay-up A with $b/t=50$.

Table 3.2 Convergence of number of terms for Layup A $[0_3/+45/90/-45]_{2s}$ with $b/t=50$, $N_{ref}=162$ and $\Delta\eta=0.025$.

σ_{FFF} [MPa]	Number of terms	Number of increments
182	3 (27)	487
125	5 (127)	348
112	7 (249)	314
108	9 (407)	304
106	11 (607)	300

The conclusions from the convergence study were that the plates with a low b/t -ratio needed a fewer number of terms than the plates with a higher b/t -ratio. Furthermore, convergence for the increment size was achieved when $\Delta\eta \leq 0.025$. The highest requirement was when the plate has a high b/t -ratio. Here, 9 numbers of terms and an increment size of 0.025 were needed to fulfil the convergence criterion. Tabulated results of parameters used for all lay-up configurations during calculation of the ULS are presented in Tables 3.3-4.

Table 3.3 Parametric values used for calculating ULS with CPDM, lay-up A $[0_3/+45/90/-45]_{2s}$.

b/t -ratio	$\Delta\eta$	Ref. load [N/mm]	Number of terms
10	0.05	5723	5 (127)
15	0.025	3801	5 (127)
20	0.025	2553	7 (249)
30	0.025	761	7 (249)
50	0.025	162	7 (249)

Table 3.4 Parametric values used for calculating ULS with CPDM, lay-up B $[-45/+45/0]_{4s}$.

b/t -ratio	$\Delta\eta$	Ref. load [N/mm]	Number of terms
10	0.05	5709	5 (127)
15	0.05	3440	5 (127)
20	0.025	2855	5 (127)
30	0.025	962	9 (407)
50	0.025	208	9 (407)

The results from the full calculations where the ULS was determined for all b/t -ratios and both lay-ups are presented and compared to Abaqus and composite PULS in Section 6.

4 Composite PULS

PULS is a software that uses the semi-analytical model programmed in Fortran 95 to reduce computational time compared to a FE analysis - an ability that was kept in mind during the development. The way PULS was developed to include composite materials is explained and motivated in Section 4.1. The results of the ULS calculations based on the developed PULS, here referred to as composite PULS, are presented and compared in Section 6.

4.1 Implementation of composite plates

The implementation process kept the approach used in PULS, which is Airy's stress function in combination with deflections to express the displacements/rotations. Failure criteria were implemented to evaluate failure and a progressive damage process was established in order to calculate the ULS. The stiffness properties of the composite plate were calculated and act as the in-data for PULS. A flowchart of composite PULS is shown in Figure 4.1, where the dotted line indicates the developed parts and the already existing PULS is located outside. The mentioned steps are described in detail in Section 4.1.1-2.

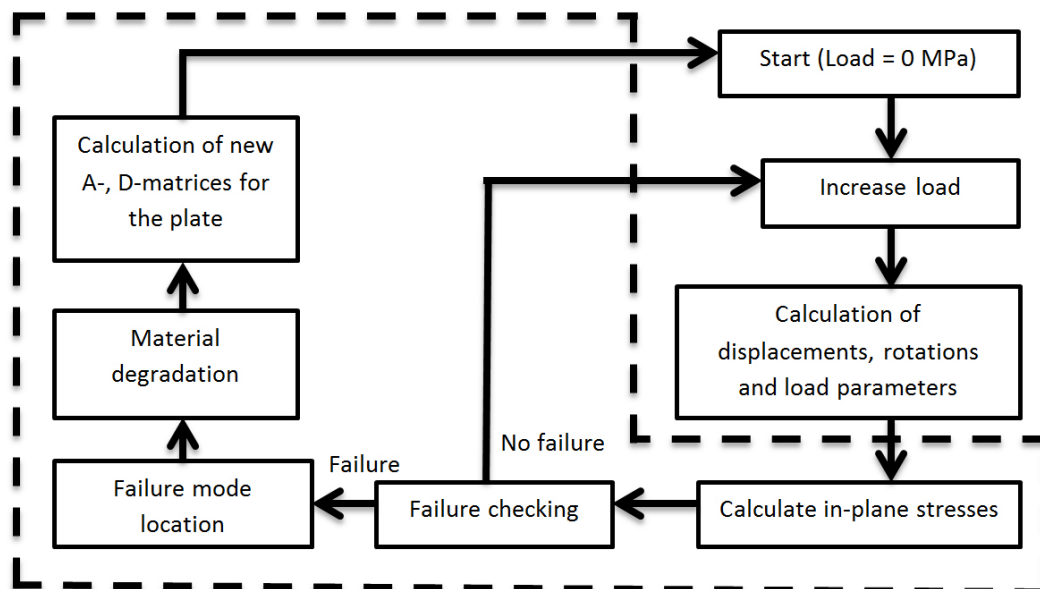


Figure 4.1 Flowchart of composite PULS accounting for FRP, where the dashed line indicates the added material into the model.

4.1.1 Implementing of composite stiffness

PULS assumes homogenous orthotropic material and in order to make this more general and extend it to account for inhomogeneous orthotropic laminates, two modifications were carried out:

- Calculation of extensional and bending stiffness matrix for the given laminate.
- Generalization of bending stiffness calculations.

The calculations of extensional and bending matrix stiffness for laminates were straightforward using theory found in basic composite mechanic literature, for example Reddy (2004) and Agarwal, et al. (2006). PULS is stress-based, whereas the extensional stiffness matrices, found in literature in this area, for the sake of simplicity use a force equilibrant. This difference means that care had to be taken when implementing the theory. The calculated extensional stiffness matrix was divided with the thickness of the plate in order to achieve the right stiffness relations for a stress approach.

A calculation of bending stiffness for a composite laminate differs from a calculation of the bending stiffness in PULS, where homogeneous material is assumed. For homogenous orthotropic materials, the bending stiffness is calculated from the known extensional stiffness matrix. To extend this calculation method, the bending stiffness matrix was calculated for the laminate and then implemented in the PULS-expression to calculate the bending stiffness. For simplicity's sake, the parts that couple the bending and twisting, the terms that include odd order derivatives, were assumed to have small effects on the final result and were thus neglected. However, the model is theoretically correct, especially for orthotropic laminates where there is no coupling between bending and twisting. Furthermore, the effect of the coupling between bending and twisting makes the material less stiff and therefore decreases the buckling load, which is non-conservative, see Jones (1999).

It has been pointed out that even small couplings between bending and twisting may cause significantly different results, see Turvey et al. (1995). Ashton (1969) studied the effect by skewing a square isotropic plate, which introduces D_{16} and D_{26} . His study showed that the effect for ratios between D_{16} and D_{11} that are small; $-0.17 < D_{16}/D_{11} < 0$, is not significant (4% decrease of the maximum out-of-plane deflection). However, for moderate ratios; $D_{16}/D_{11} \approx 0.5$, the effect is significant (24% decrease of the maximum out-of-plane deflection).

The bending stiffness has an impact on the bending energy, and, in order to show the difference, the equation of bending energy for homogenous orthotropic material derived in Byklum (2002) Equation (4.1) was compared with the one taking laminates, into account, Equation (4.2).

$$U^b = \frac{t^3}{24} \int_A (C_{1111} w_{,11}^2 + 2C_{1122} w_{,11} w_{,22} + C_{2222} w_{,22}^2 + 4C_{1212} w_{,12}^2) dA \quad [\text{Nm}] \quad (4.1)$$

$$U^b = \int_A (D_{1111} w_{,11}^2 + 2D_{1122} w_{,11} w_{,22} + D_{2222} w_{,22}^2 + 4D_{1212} w_{,12}^2) dA \quad [\text{Nm}] \quad (4.2)$$

where C_{xxxx} is the stiffness matrix for homogenous material, D_{xxxx} is the bending stiffness matrix components and $w_{,xx}$ is the deflection differentiated in a different direction indicated by “,”. The difference is that the homogenous material in Equation (4.1) is independent of the thickness and the term $t^3/24$ can be extracted from the integral. For laminates, the thickness needs to be included in the calculation of the bending stiffness matrix.

4.1.2 Calculation of in-plane stresses and failure degradation

In order to calculate the load-carrying capacity past FPF, it was necessary to introduce a progressive damage model. A CDM-model is often found in articles, see Garnich et al. (2009), Maimi et al. (2007), Hu et al. (2010), where one reason is that the method offers various degrees of complexity depending on the analysis type. An instantaneous degradation model with a constant degradation factor is conservative and computationally fast. On the other hand, Garnich et al. (2009) argue that a progressive failure analysis of a composite structure should use gradual degradation in order to reflect the actual failure process. The downside with the gradual degradation is the computational cost, since the stiffness matrices are continuously changing, which is not suited to a simplified method. Models based on the fracture mechanics method become complex in order to define crack growth paths, crack growth rates or crack profiles necessary for the calculations, see Hu et al. (2010). With regard to the investigated progressive failure analysis the simplest method, the CDM-model with instantaneous degradation, was implemented in PULS. The stiffness matrix is degraded to 1 % of its initial stiffness with regard to the detected failure mode.

There are several different failure criteria described for composite, and in PULS the Hashin-Rotem criteria were used. The reason for choosing these particular criteria was that the failure mode is clearly stated. The Hashin-Rotem are recognized criteria and CPDM uses these criteria making the two models comparable. It is also beneficial to know the failure mode in order to degrade the correct material property upon failure. Mode-independent criteria would need assumptions to be made in order to determine which failure mode that occurs. Furthermore, the complexity of the Hashin-Rotem criteria is low, since these use few terms and easily accessible material properties. The Hashin-Rotem criteria are easy to implement and they are the default failure criteria in Abaqus allowing for further comparisons.

It is mentioned in Section 2.3.1 that delamination is a vital failure mode in composite structures, mainly caused by inter-laminar shear contributions. Hashin-Rotem failure criteria do not consider this failure mode, and other criteria in order to determine this failure mode have not been considered. The reason for this is that the PULS-theory disregards out-of-plane shear contributions, and only considers in-plane shear, which is represented in the Hashin-Rotem failure criteria. Knowing the failure mode for the laminates allowed degradation of this specific element and further calculation was evaluated in order to find the ULS. To detect if failure has occurred, the stresses in each ply are needed.

The calculation of stresses in each ply is relevant for checking if failure occurs in the laminate, where membrane strains and curvature of the plate are essential. Curvatures are not of the same importance for steel plates, which are governed by the membrane strains. For this reason curvatures are not implemented in PULS, while they had to be implemented into composite PULS. The curvatures are calculated using Kirchhoff's assumptions, which give functions dependent on differentials of the out-of-plane displacement, see Appendix A. Since the out-of-plane displacement is well defined in PULS, the curvatures were found by differentiating this expression with regard to x and y . Kirchhoff's assumptions were used because of the simplicity. However, they resulted in a stiffer material since shear deformation is restricted compared with a

theory applying a first-order or higher order of shear deformation theory. This choice of assumptions will have a non-conservative effect on thicker plates, while the effect on thinner plates will be small; see Agarwal et al. (2006). With the curvature and the membrane strain defining the ply strain, the in-plane stresses in each ply can be calculated, see Equation (4.3)

$$\begin{Bmatrix} \sigma_x \\ \sigma_y \\ \tau_{xy} \end{Bmatrix} = \begin{bmatrix} \bar{Q}_{11} & \bar{Q}_{12} & \bar{Q}_{16} \\ \bar{Q}_{12} & \bar{Q}_{22} & \bar{Q}_{26} \\ \bar{Q}_{16} & \bar{Q}_{26} & \bar{Q}_{66} \end{bmatrix}_k \left(\begin{Bmatrix} \varepsilon_x^0 \\ \varepsilon_y^0 \\ \gamma_{xy}^0 \end{Bmatrix} + z \begin{Bmatrix} k_x \\ k_y \\ k_{xy} \end{Bmatrix} \right) \text{ [MPa]} \quad (4.3)$$

The degradation of the laminate is a minor alternation of the degradation process proposed by Yang (2013). PULS has no coupling between strain and curvature, i.e. the coupling matrix $\mathbf{B}=0$, which means that asymmetry in the lamina was not considered.

In order to keep the model conservative, the degradation model was altered to make symmetric degradation implying that if matrix failure occurs in the top ply, degradation will be performed in both top and bottom in order to maintain symmetry in the laminate.

5 Finite element analysis

To validate the results given by CPDM and composite PULS, a parallel study using finite element analysis was performed. The FE-program used was Abaqus Standard 6.12, see Abaqus (2012). In the following text a model description in addition to the analysis procedure is presented. Further, a mesh study was carried out and the calculated ULS results are presented in Section 6.

5.1 Abaqus model and material set-up

The first step in creating the model was to define the geometry. A square plate with the desired measurements, see Section 1.4, was modelled in two dimensions, defined as a deformable planar shell. Since the thicknesses are significantly smaller than the remaining dimensions, the shell assumption was considered valid. The material properties, including failure criteria and the damage evolution model, needed to be expressed in order to create the composite lay-up. With the defined part and material properties, the composite lay-ups were created, choosing the number of plies, fibre directions, materials, integration method as well as the number of integration points through each ply.

5.2 Boundary conditions and loadings

The boundary conditions were kept simply supported around the edges, see Table 5.1, for all cases, and the loads were varied from a uniaxial to a biaxial compression.

Table 5.1 *Simply supported boundary conditions where the length = a, and the breadth = b, U is displacement.*

Boundary conditions, simply supported			
x=0	x=a	y=0	y=b
U3=0	U1=U3=0	U3=0	U2=U3=0

A reference point was established outside the plate geometry, in which the loads were applied. The two edges that were free to move in their respective directions, see Figure 5.1, were coupled to the reference point formed as sets, meaning that the edge remained straight when subjected to loads. The coupling between the reference point and the sets was established through two constraints. Since the edges were free to rotate during loading, it was desired for the loads to act normal to the edge during rotations.

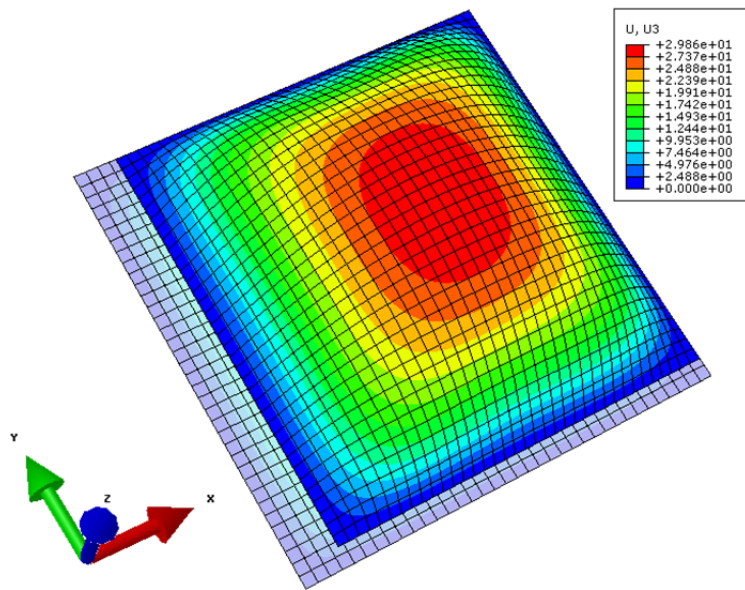


Figure 5.1 Lay-up A subjected to a compressive load in the x-direction, showing out-of-plane displacement. Two edges are free to move in their respective directions, indicated by the light blue area. The deformations are scaled with a factor of 10.

5.3 Damage evolution

The damage evolution model in Abaqus was defined by the energy release rate in four loading conditions; longitudinal tensile and compressive loading and transverse tensile and compressive loading. The degradation was linear, and the input in Abaqus required four critical energy release rates, where each of the critical energy release rates match the area of the large triangle, see Figure G.1, for the respective loading conditions. The critical energy release rate-inputs were calculated using the equations found in Appendix G.

The reason for expressing the model in terms of equivalent stresses and strains was to avoid the strong mesh dependency by introducing the term L^C . L^C is the length between two nodes for the chosen elements.

The failure criteria available in Abaqus are Hashin-Rotem and Hashin. The main difference is the out-of-plane shear contribution, which was expected to have an effect on the matrix failure, see Section 2.3.5. In order to reflect the models presented in Sections 3 and 4, the Hashin-Rotem failure criteria were applied in Abaqus. Both composite PULS and CPDM use the Hashin-Rotem criteria. In this way the differences caused by the theories between the models can be detected. The inputs in Abaqus were the material strengths presented in Table 1.1. A minor study was carried out to see the differences of the ULS for the Hashin-Rotem and Hashin failure criteria, where the ULS calculated ones were unaffected by which criteria that were chosen. These results can be seen in Appendix I, Table I.1.

5.4 Analysis procedure

The analysis was divided into two processes. The first process was a static stress/displacement analysis in order to estimate the bifurcation load, which was done by the linear perturbation method. From this analysis the preferred buckling mode was found by the first eigenvalue, and the mode-shape was used as input in the next analysis as an initial geometric imperfection of the plate. The geometric imperfection similar to the first natural buckling mode is known to cause the lowest ULS, see Misirlis (2012). The displacement from the linearized eigenvalue analysis was written in the *Edit Keywords* with the following term: *NODE FILE U. The creation of an initial imperfection is important in order to get a continuous response prior to the post-buckling behaviour.

The bifurcation load was expressed as:

$$P^N + \lambda_i Q^M = 0 \text{ [MPa]} \quad (5.1)$$

where N and M are the degrees of freedom (DOF), P is the preload, Q is the perturbation load and λ is the eigenvalue. By multiplying the perturbation load and the first eigenvalue, the external load to cause buckling was found.

The next process was to analyse the load-displacement behaviour of the material. There were both material and geometric non-linearities and due to these non-linear aspects the Static Riks method was chosen as analysis type in Abaqus. Static Riks is an incremental solution based on the arc length method. An automatic increment scheme was used in order to ensure high computational efficiency. The initial arc length increment was varied between 0.1 and 1, while the minimum increment was equal to 10^{-7} . A load proportionality factor (LPF) was found at each increment. The initial imperfection found by the linear perturbation method was implemented in the *Edit Keywords* option with the input-file: *IMPERFECTION, FILE="name-of-the-job", STEP=1, 1, w. The letter w is the maximum amplitude of the initial imperfection, here defined as 0.1% of the breadth.

An analysis was done without failure initiation in order to check for reasonable results of both the lay-ups, and further compared against both composite PULS and CPDM. The load-displacement curves can be seen in Section 6.1.

5.5 Element type

For a 2D planar shell model the following types of conventional elements are available in Abaqus: four-node linear quadratic shell elements (S4R), eight-node non-linear quadratic shell elements (S8R) and three-node triangular shell elements (S3R). For these element types there are different configurations depending on the type of analysis. The triangular element was excluded at an early stage since it only calculates thin plate solutions. The remaining elements are briefly presented below. Only elements with reduced integration were considered. The reason for using reduced integration was that the computational time is significantly reduced compared to fully integrated elements, while the accuracy of the results remains the same, see Abaqus (2012).

The S8R element is an eight-node second-order quadratic shell element that can be expressed with five or six DOF; three displacement and two/three rotations. With five DOF the element is limited to “thin-shell” theory neglecting out-of-plane shear contributions, and solutions for thicker plates are therefore expected to be inaccurate. With six DOF the shell element handles out-of-plane shear contribution for the plates, where this contribution is less vital for thin plates. As the element has eight nodes, the large deflections of the plate can be described accurately with fewer elements compared to a linear element type.

The S4R element is a four-node linear element that treats finite membrane strains or small strains with large rotations. The small strain set-up is limited to five DOF, and was rejected for the same reason as the S8R5 elements. The S4R element that deals with finite strains includes out-of-plane stress in order to analyse thick plates. Since the element-type is linear, smaller elements compared to the non-linear type are necessary in order to describe larger displacements.

The choice was between S4R- and S8R-elements, both with 6 DOF, and an analysis was performed in order to see the difference in the solutions for a thin plate, see Figure 5.2.

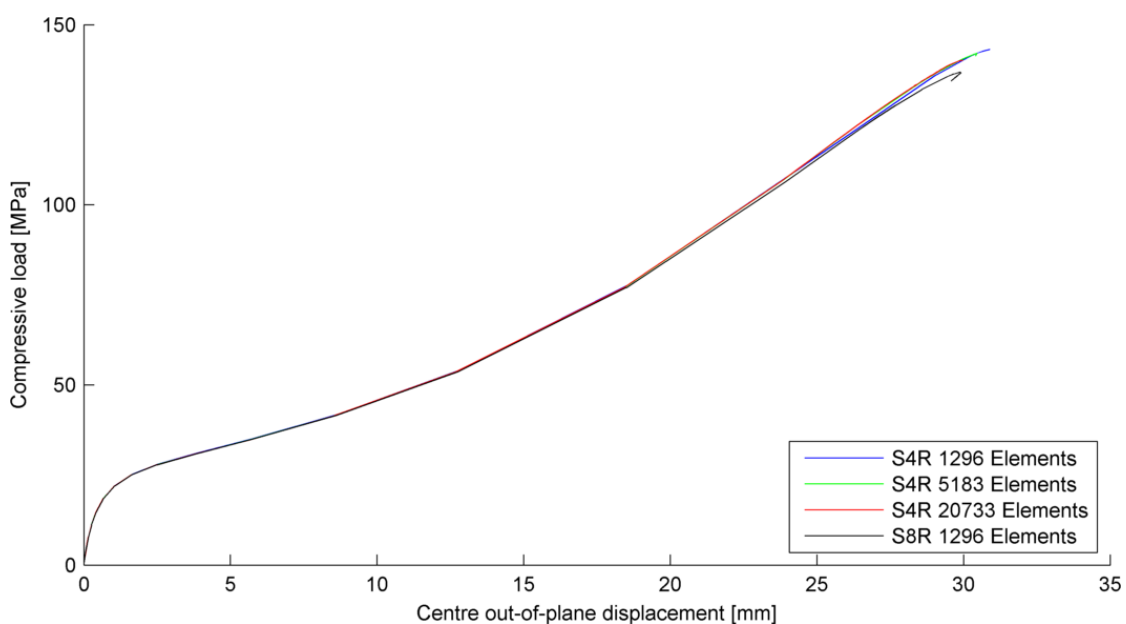


Figure 5.2 Load-displacement relation for different element-types.

From this study, the curves fit well and only small differences regarding the ULS were found. The S8R element type gave the most conservative solution, approximately a 2 % lower ULS-load. The number of elements was varied for the S4R element, see Figure 5.2, and the trend was that the ULS converged against the ULS value calculated for S8R with fewer elements, see Figures 5.3 and 5.4. On the other hand, the computational time increased significantly when more elements were required. For this reason, the S8R elements were found to give faster and more reliable solutions and became the choice of element type in the calculations. Furthermore, in order to describe the cross-sectional behaviour of the chosen shell element, Simpson’s integration rule with three section points in each ply was applied.

Simpson's integration rule was used in order to determine transverse shear stress in the interface between the plies.

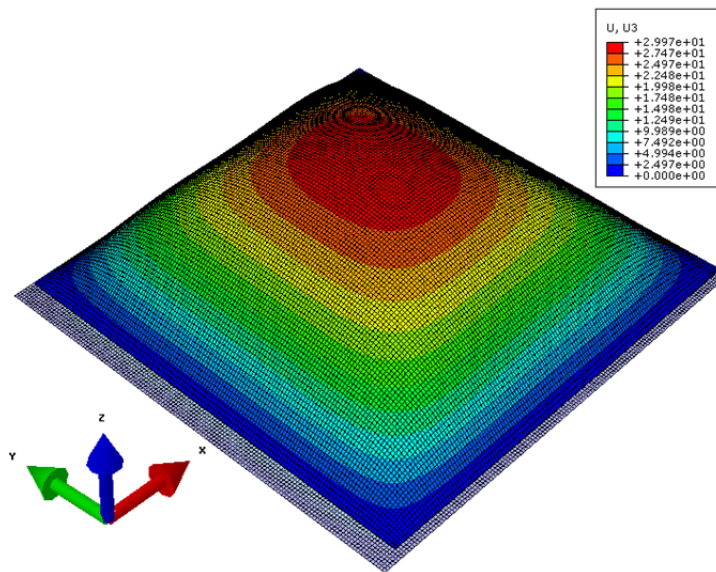


Figure 5.3 *Lay-up A subjected to uniaxial compressive loads, 20733 S4R elements, showing out-of-plane displacement. The shaded area along two of the edges indicates the displacement from the original shape. The deformations were scaled with a factor of 5 in all directions.*

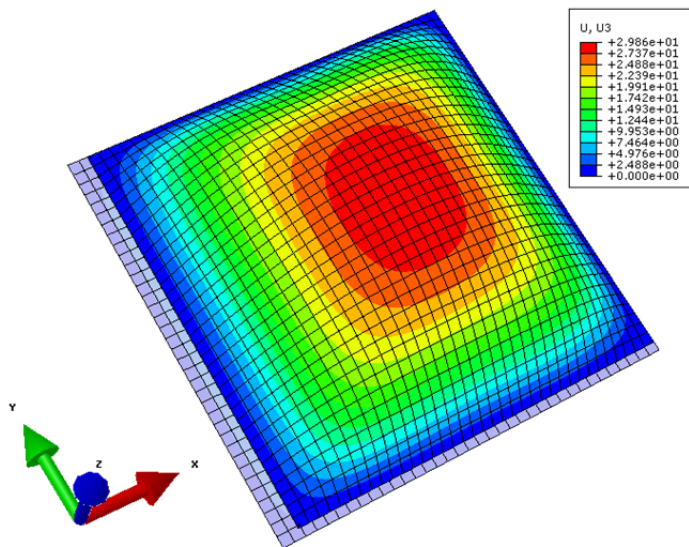


Figure 5.4 *Lay-up A subjected to uniaxial compressive loads, 1296 S8R elements, showing out-of-plane displacement. The shaded area along two of the edges indicates the displacement from the original shape. The deformations were scaled with a factor of 5 in all directions.*

5.6 Mesh convergence study

A mesh convergence study was done to establish the number of elements needed for a converged result. This was done stepwise by calculating the ULS for the following number of elements, for the thinnest and the thickest plate, $b/t=50$ and $b/t=10$ respectively:

- 100 elements
- 400 elements
- 900 elements
- 1024 elements
- 1296 elements
- 1600 elements
- 2116 elements

Both the ULS and the load proportional factor (LPF) from the static Riks analysis and the first buckling load for each element size were checked. The LPF is a magnitude, which, decomposed, describes the load in the longitudinal and transverse directions.

In Figures 5.5 and 5.6 the ULS-load has been plotted against a varied number of elements for the plates with highest and lowest b/t ratio, respectively, for both the lay-ups subjected to uniaxial loading. The differences were smaller for lay-up A compared to lay-up B, which resulted in converged results for a fewer number of elements. The exact values can be seen in Tables H.1-H.4.

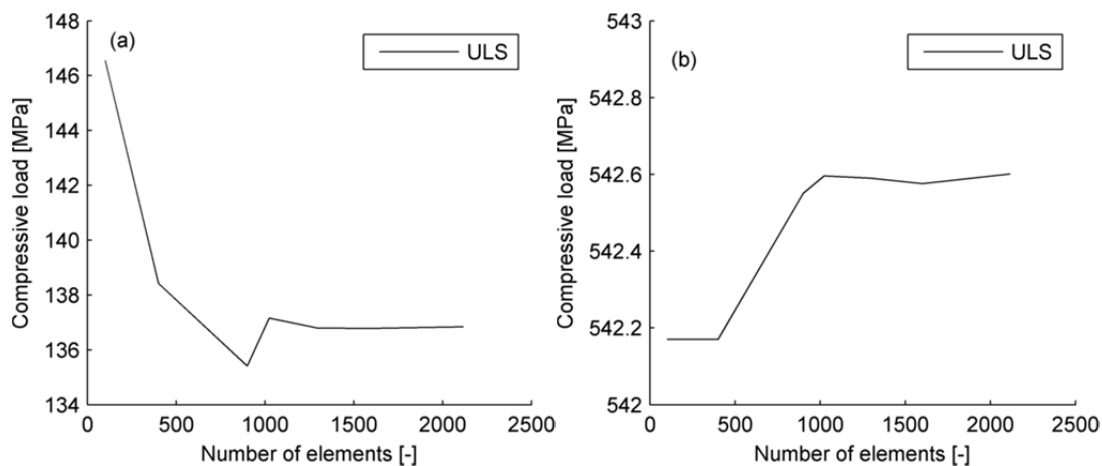


Figure 5.5 ULS-load – number of elements for lay-up A $[0_3/+45/90/-45]_{2S}$, with (a) $b/t=50$ and (b) $b/t=10$.

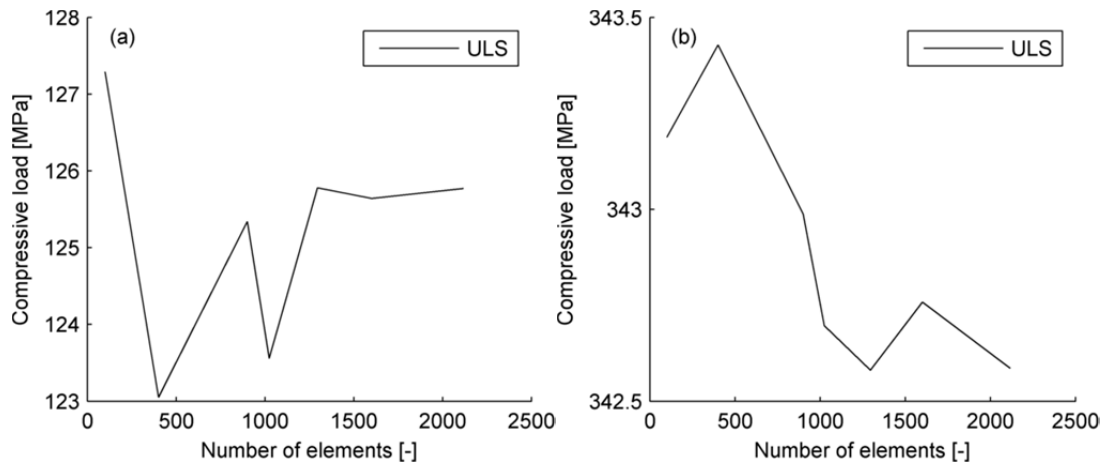


Figure 5.6 ULS-load – number of elements for lay-up B $[-45/+45/0]_{4S}$, with (a) $b/t=50$ and (b) $b/t=10$.

In order to check mesh convergence for the plates subjected to biaxial loadings, the LPF was plotted against a varied number of elements in the same way as for uniaxial loading, presented in Figures 5.7 and 5.8. The load-ratio that was used in the convergence study for biaxial loads, was $\frac{N_x}{N_y} = 0.84$. As for the uniaxial load-case,

lay-up B needed a higher number of elements in order to have converged results. An additional study using 3200 elements was necessary for lay-up B in order to ensure convergence.

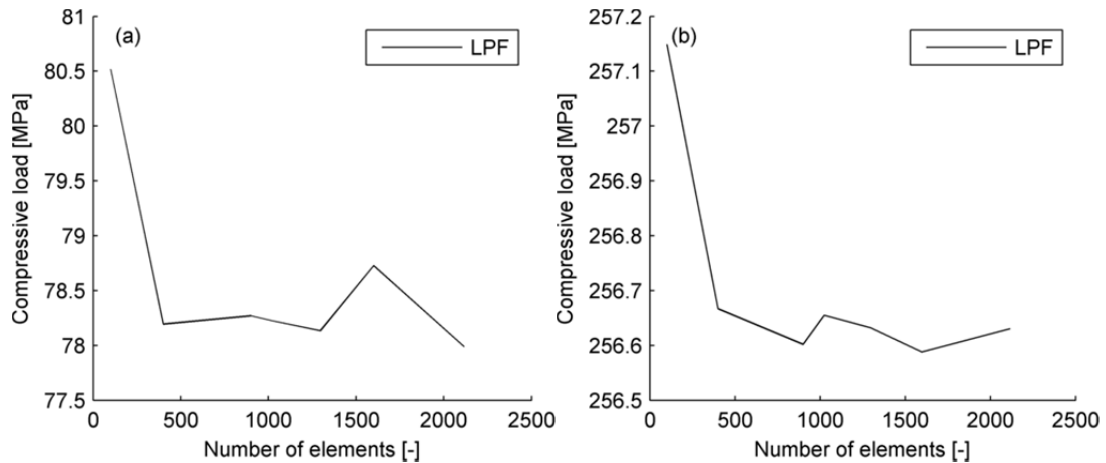


Figure 5.7 LPF – number of elements for lay-up A $[0_3/+45/90/-45]_{2S}$, with (a) $b/t=50$ and (b) $b/t=10$.

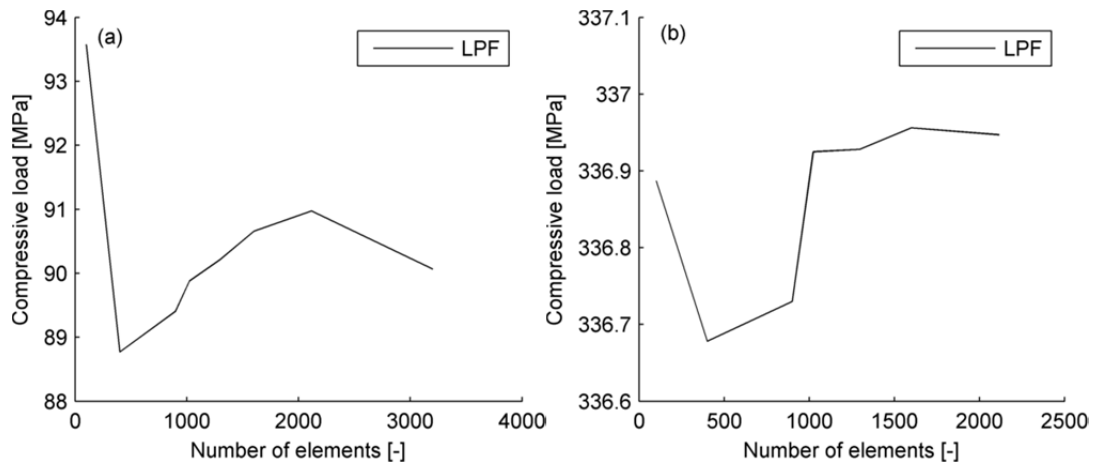


Figure 5.8 LPF – number of elements for lay-up B $[-45/+45/0]_{4S}$, with (a) $b/t=50$ and (b) $b/t=10$.

A more general check including the entire load spectrum vs centre out-of-plane displacement showed that the curve had a good fit from 900 elements and more, see Figure 5.9. Only with 100 and 400 elements, did the curve show a visible divergence in the ultimate failure area.

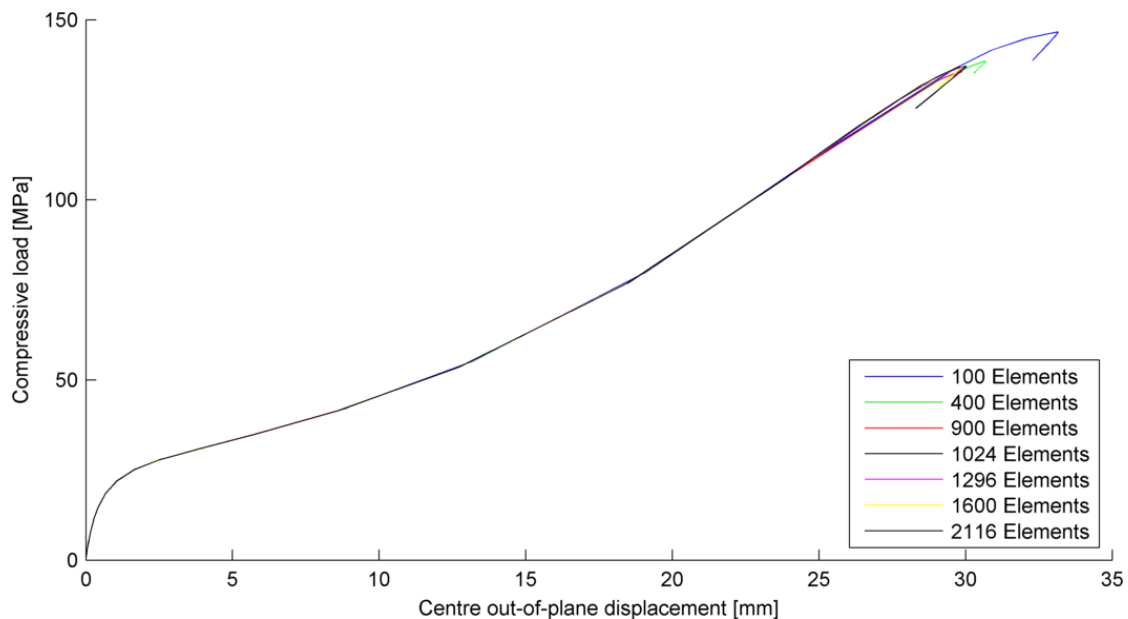


Figure 5.9 Mesh refinement, plate A $[0_3/+45/90/-45]_{2S}$, $b/t=50$.

In order to ensure that the elements were sufficiently small a mesh convergence study was performed for the plates with the highest and lowest b/t ratio of both the lay-ups. The exact values are available in Tables H.1-H.4 in Appendix H. In general, the results were good enough with 900 elements, only with a few exceptions. With 1,296 elements all the study-cases showed converged results. The difference in computational time between a mesh of 900 elements compared to 1296 elements was minor. Instead, there was more time to save, during model-making, in applying a standard mesh for all the models.

6 Comparison and discussion of postbuckling analyses

Section 6 presents, compares and discusses some of the results calculated by composite PULS, CPDM and Abaqus, the remaining results can be found in Appendix I.

The structure of this section consists of four parts, the first part discusses the ability to describe the out-of-plane displacement due to the load. In order to discuss the displacement description of the different models, the comparison was made by calculating the deflection of the plate without failure or degradation. The second part discusses the relation between ULS calculated for each model under uniaxial loads. In the third part, biaxial loads are compared and discussed and in the final part the consequences of not accounting for delamination are briefly discussed.

6.1 Displacement description without failure

In order to verify that the material properties were implemented correctly, load-displacement curves without failure or material degradation were plotted. Furthermore, the effects of not implementing the first-order shear deformation theory (FSDT) into PULS were evaluated and compared with the results gained from CPDM. Four plots of load-displacement curves without failure are presented in Figures 6.1-6.2.

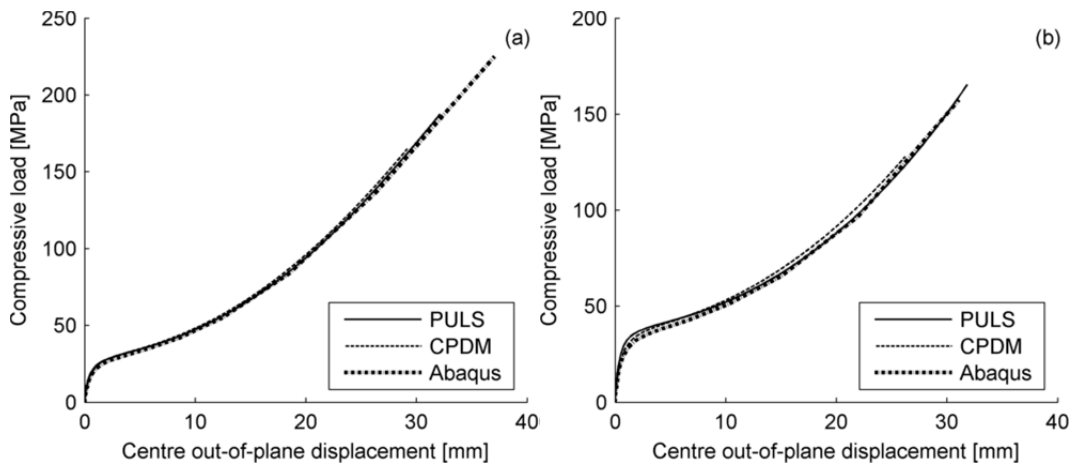


Figure 6.1 Load-displacement curves without failure for lay-up A $[0_3/+45/90/-45]_{2S}$ (a) and lay-up B $[-45/+45/0]_{4S}$ (b), both with $b/t=50$.

Both CPDM and composite PULS show a good fit for the load-displacement relation for the thin plates, see Figure 6.1. The reason for this good correlation, despite the restraints from the assumptions involved by the theories of the classical laminated plate theory (CLPT) and FSDT, is believed to be due to the high b/t ratio. The high b/t -ratio resulted in a negligible out-of-plane normal stress and shear stress contribution, and the theories without this contribution, or only a first-order contribution, would give the same results. However, for plates with lower b/t ratios, where the out-of-plane shear contribution was not negligible, the load-displacement relation shows a stiffer plate for the simplified theories, see Figure 6.2. With this

relation in mind, the focus of Section 6.2-6.3 is on the effects caused by different progressive failure methods from the first ply failure (FPF) until the ULS.

Despite the good correlation seen in Figure 6.1, some deviation is still present. The reason for this deviation is that the load-displacement curves, for both composite PULS and CPDM, were found using the Rayleigh-Ritz method in combination with the perturbation method. The perturbation method operates with small linear increments where the non-linear contribution from the large deflection theory is linearized. This linearization results in a small “over-shooting” when the change in deflection is great, see Figure 6.1(b) around 30 MPa.

In Figure 6.2, composite PULS clearly shows weaknesses when calculations were made for plates with lower b/t -ratios, which is due to the fact that CLPT disregards the out-of-plane stress contributions. The better approximation from CPDM is because the out-of-plane shear deformation contribution is accounted for through FSDT. The differences are visible for both lay-ups with $b/t=10$, although for lay-up B the CPDM-curve is located somewhat closer to PULS than to Abaqus. Why CPDM does not match Abaqus better is not known, and some deviation was expected due to the perturbation method but when smaller increments were tried there was no noticeable difference.

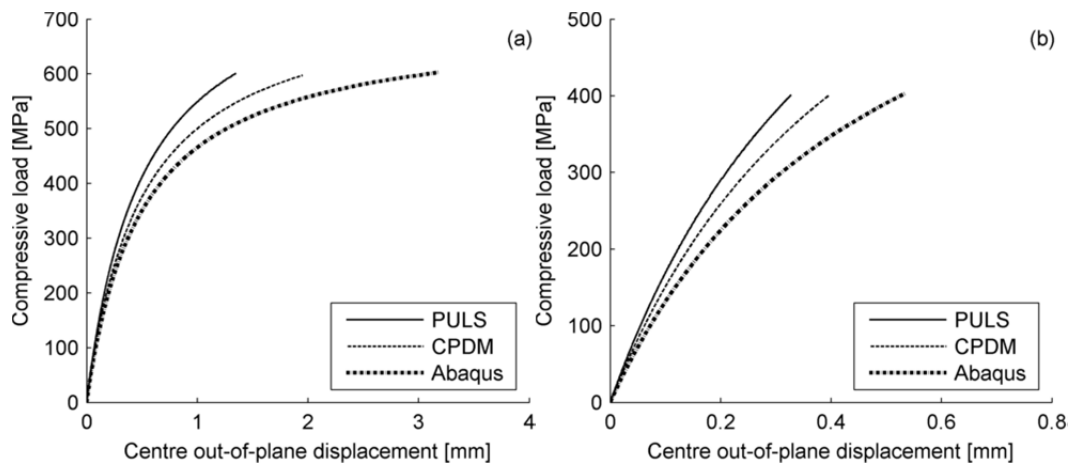


Figure 6.2 Load-displacement curves without failure for lay-up A $[0_3/+45/90/-45]_{2S}$ (a) and lay-up B $[-45/+45/0]_{4S}$ (b), both with $b/t=10$.

6.2 Uniaxial load cases

In this section, the failure and the degradation model were implemented in the load-displacement calculations. Figures 6.3-6.6 illustrate the results of the calculations with composite PULS, CPDM and Abaqus. Furthermore, the first buckling load was calculated as a reference to the ULS.

The differences between the models were shown to initiate after FPF, and therefore the discussion focuses on this part. Abaqus degrades the material properties linearly, which means that the degradation affects the stiffness of the plate more slowly compared to composite PULS and CPDM which instantaneously degrade the complete ply. It is assumed that the ply in reality has residual strength in the

remaining undamaged parts of the ply and for this reason the linear degradation model in Abaqus is more accurate compared to the instantaneous complete ply degradation.

The reason for the cluttered load-displacement curves for both CPDM and composite PULS, see Figure 6.3, is that the calculations of displacements and curvatures were restarted from an unloaded condition after each degradation. The load-displacement curves are therefore plotted for all calculated values up to FPF, and, from this point on, only the failure points from each reloading were indicated. This means that the load-displacement curves are somewhat overestimated between the failure points, while the ULS and all failure points are precise. Tabulated results are presented in Tables 6.1-6.3, for lay-up A and B where FPF and first fibre failure (FFF) for composite PULS and Abaqus are specified.

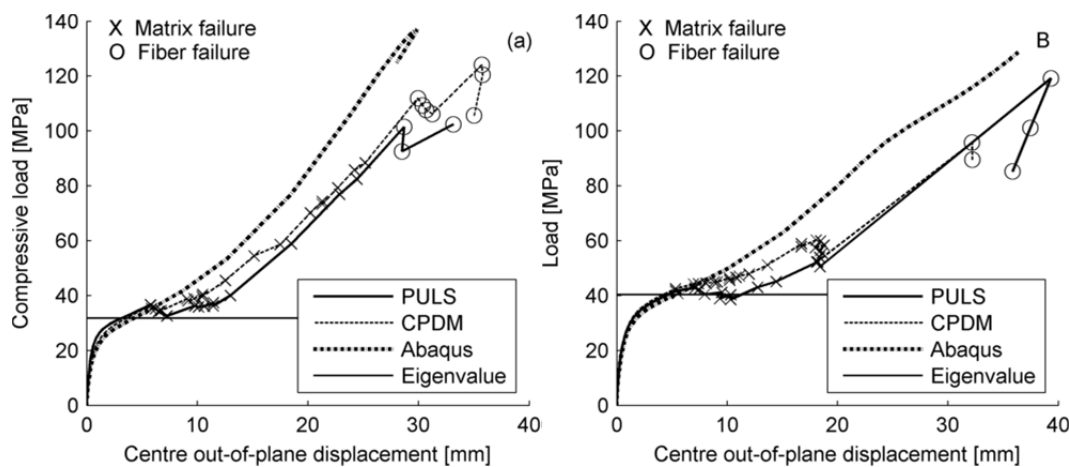


Figure 6.3 Load-displacement curves for lay-up A $[0_3/+45/90/-45]_{2S}$ (a) and lay-up B $[-45/+45/0]_{4S}$ (b), both with $b/t=50$.

In traditional standard ULS design, the ULS is located at the first buckling load or FPF, see DNV (2013 a). Compared to this design criterion, the plates with a b/t -ratio of 50 show a significant residual strength after both FPF and the first buckling load, see Figure 6.3. Composite PULS calculates the maximum load-carrying capacity independent of the failure sequence, which means that several fibre failures could occur before the ULS is reached. Fibre failure in tension can be rather violent and the dynamics of such a failure could cause immediate total failure. Since the ultimate strength is considered as the maximum load-carrying capacity, the results can be non-conservative in occasions with multiple fibre failures.

As the b/t -ratio was decreased, the FPF occurred for loads lower than the first buckling load, but there is still a residual strength in the laminate. For the thickest plates considered in this thesis, the first buckling load was found to be much larger than the collapse load. This implies that for plates with low b/t -ratios the non-linear terms in the large deflection theory could be disregarded, since the maximum load is reached when the deflection is small compared to the thickness, Turvey et al. (1995). If the large deflection theory may be disregarded, the semi-analytical methods do not require a perturbation method in order to estimate the ULS.

The comparison between Abaqus and composite PULS was performed in detail where the plies degraded for FPF and FFF were investigated. The expectation was to find that the same plies were degraded for the FPF for composite PULS and Abaqus, since no degradation has occurred before FPF. However, some variation for the FFF could be expected due to the different degradation models, where composite PULS utilizes complete ply degradation, which affects the load distribution in the laminate. Tables 6.1-6.3 show that this was expected for most cases, although for the plates with the lowest b/t -ratio this was not the case. The reason for FPF in different plies is believed to be related to the predominate end shortening in the longitudinal direction. The FPF for composite PULS occurred within a reach of 96% to 104% of the FPF calculated with Abaqus. For both plates with a b/t -ratio of 50, the FPF occurs after the first buckling load.

Table 6.1 Overview FPF [MPa] and FFF [MPa], Lay-up A $[0_3/+45/90/-45]_{2S}$. The numbers in the parenthesis indicate the fiber direction. The subscript P indicates composite PULS and the subscript A indicates Abaqus.

	Composite PULS				Abaqus			
b/t	Ply	$\sigma_{FPF.P}$	Ply	$\sigma_{FFF.P}$	Ply	$\sigma_{FPF.A}$	Ply	$\sigma_{FFF.A}$
10	5(90°)	298	1(0°)	437	20(90°)	292	1(0°)	539
30	24(0°)	83	21(45°)	157	24(0°)	80	21(45°)	187
50	24(0°)	36	21(45°)	101	24(0°)	35	21(45°)	122

Table 6.2 Overview FPF [MPa] and FFF [MPa], Lay-up B $[-45/+45/0]_{4S}$. The numbers in the parenthesis indicate fiber direction. The subscript P indicates composite PULS and the subscript A indicates Abaqus.

	Composite PULS				Abaqus			
b/t	Ply	$\sigma_{FPF.P}$	Ply	$\sigma_{FFF.P}$	Ply	$\sigma_{FPF.A}$	Ply	$\sigma_{FFF.A}$
10	22(0)	162	3(0°)	303	N/A(*)	N/A(*)	3(0°)	342
30	24(0)	85	4(-45°)	163	24(0°)	89	2(45°)	161
50	22(0)	42	1(-45°)	119	22(0°)	41	2(45°)	124
(*) N/A = No answer								

Table 6.3 A comparison of the loads from Table 6.1 and 6.2. The subscript P indicates composite PULS and the subscript A indicates Abaqus.

b/t	Lay-up A		Lay-up B	
	$\frac{\sigma_{FPF.P}}{\sigma_{FPF.A}}$	$\frac{\sigma_{FFF.P}}{\sigma_{FFF.A}}$	$\frac{\sigma_{FPF.P}}{\sigma_{FPF.A}}$	$\frac{\sigma_{FFF.P}}{\sigma_{FFF.A}}$
10	1.02	0.81	N/A(*)	N/A(*)
30	1.04	0.84	0.96	1.01
50	1.03	0.83	1.02	0.96
(*)N/A = No answer				

The ULS calculated with composite PULS were in most cases similar or slightly lower than the results from CPDM, see Table 6.4 and 6.5. The reason for the slightly smaller ULS is the symmetric complete ply degradation that composite PULS uses. In two cases, the lay-up B b/t -ratio equal to 50 and 30, composite PULS calculates less conservative ULS compared to CPDM. The small difference for the plate with a b/t -ratio of 30 can be explained by the disregarded coupling between bending and twisting (the difference in ULS is about 4%).

Table 6.4 Overview ULS [MPa], Lay-up A $[0_3/+45/90/-45]_{2S}$

b/t	CPDM $\sigma_{ULS,C}$	Composite PULS $\sigma_{ULS,P}$	Abaqus $\sigma_{ULS,A}$	$\frac{\sigma_{ULS,P}}{\sigma_{ULS,A}}$	$\frac{\sigma_{ULS,C}}{\sigma_{ULS,A}}$
10	484	490	543	0.90	0.89
15	273	276	306	0.90	0.89
20	205	208	259	0.80	0.79
30	166	157	215	0.73	0.77
50	124	102	137	0.74	0.91

Table 6.5 Overview ULS [MPa], Lay-up B $[-45/+45/0]_{4S}$

b/t	CPDM $\sigma_{ULS,C}$	Composite PULS $\sigma_{ULS,P}$	Abaqus $\sigma_{ULS,A}$	$\frac{\sigma_{ULS,P}}{\sigma_{ULS,A}}$	$\frac{\sigma_{ULS,C}}{\sigma_{ULS,A}}$
10	305	303	343	0.88	0.89
15	281	280	298	0.94	0.94
20	204	200	220	0.91	0.93
30	140	146	162	0.90	0.86
50	96	119	129	0.92	0.74

The big difference for the highest b/t -ratio cannot solely be explained with the neglected coupling relation. The effect on the ULS from the coupling terms was investigated by running CPDM with $D_{16} = D_{26} = \mathbf{B} = 0$. The calculation resulted in a higher ULS (103.7 MPa), but it was still far from the result gained by composite PULS. There are two additional differences between composite PULS and CPDM; Composite PULS disregards shear deformations and the stresses are calculated from a Fourier series expressing the deflection. Since the deflections are closely matched, see Figure 6.1(b), it indicates that the disregarded shear deformations do not affect the deflection. The reason for the difference between the ULS results for composite PULS and CPDM should then be due to the different methods of stress calculations. In order to investigate if the number of terms for composite PULS affected the result, an additional calculation was made with 15 number of terms instead of 10. The increase in the number of terms had no effect on the ULS result.

For a decreasing b/t -ratio, the accuracy of the semi-analytical load-displacement curves deteriorated before FPF, see Figure 6.4, which this is due to the perturbation method. The gap between composite PULS and CPDM in the range between a displacement of 5 – 20mm, was caused by the additional loss of matrix strength due to the symmetrical degradation. In the range where the residual strength is mainly carried by the fibres, the curves of the semi-analytical models agree.

In Figure 6.4(a), CPDM indicates more than one fibre failure before reaching the ultimate strength, while composite PULS defines the ultimate strength at the first fibre failure. The reason for this difference in ultimate strength is that the residual strength after symmetric fibre degradation is too small to contribute to any further load increase.

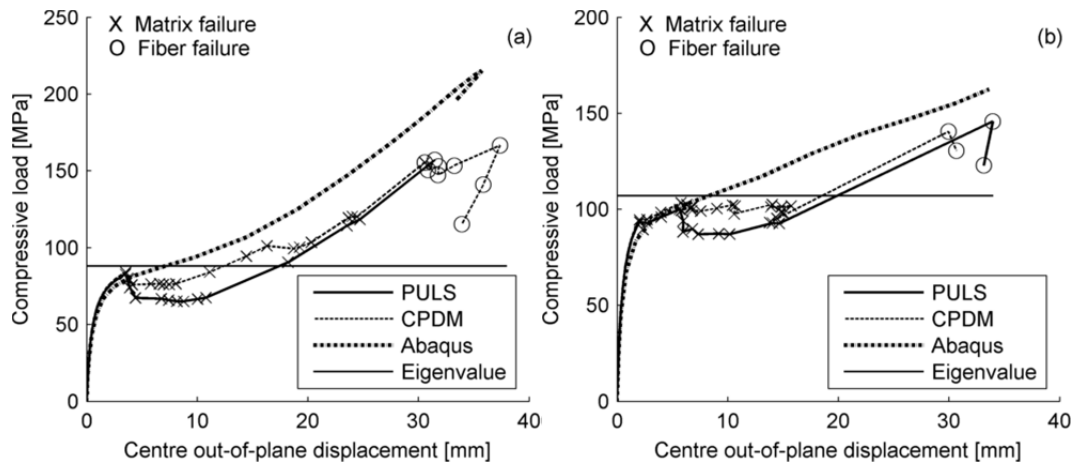


Figure 6.4 Load-displacement curves for lay-up A $[0_3/+45/90/-45]_{2S}$ (a) and lay-up B $[-45/+45/0]_{4S}$ (b), both with $b/t=30$.

For the plates with the lowest b/t ratio, see Figure 6.5, absolute failure occurs for loads significantly lower than the first buckling load. The reason for failure before the first buckling load is that the plates, due to their b/t ratio, are too stiff to buckle, which results in material failure before buckling occurs. However, it must be noted that the stiffness predicted by composite PULS is greater than for CPDM, even though degradation is performed symmetrically for composite PULS. The reason for this greater stiffness is that CPDM calculates with FSDT taking shear deformation into account, allowing the material to deform in out-of-plane shear.

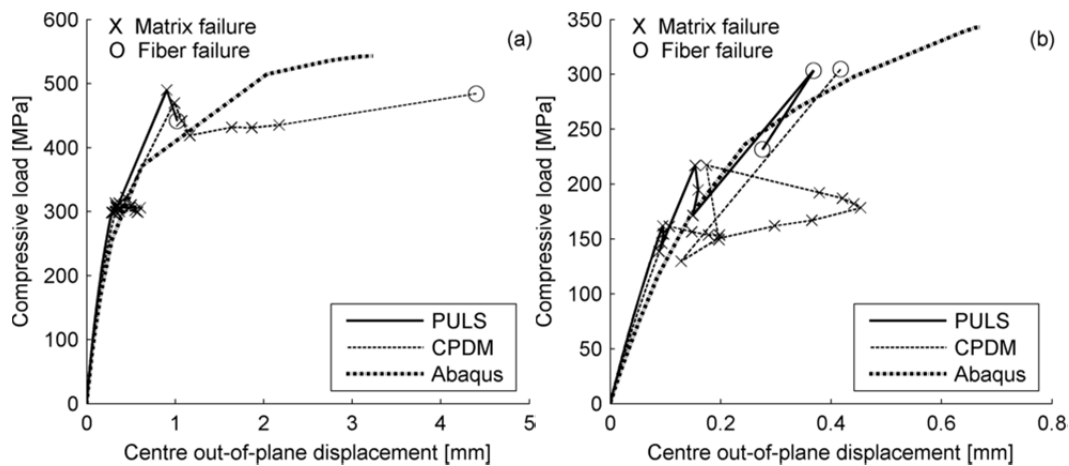


Figure 6.5 Load-displacement curves for lay-up A $[0_3/+45/90/-45]_{2S}$ (a) and lay-up B $[-45/+45/0]_{4S}$ (b), both with $b/t=10$.

By following the “x” in the CPDM curve in Figure 6.5(b), the bending stiffness seems to increase from degradation for the plates with the lowest b/t ratio, especially the lay-up B $b/t=10$. The bending stiffness reduction can seem peculiar, since it indicates that the material becomes stiffer from degradation. However, the deflection is small for the plates with the lowest b/t -ratio and the load-displacement curve expressed by longitudinal end-shortening presents the result more clearly, see Figure 6.6. A closer investigation showed that the first failures occurred at the top of the plate, which resulted in an unsymmetrical degradation for CPDM. The unsymmetrical degradation

made the plate less sustainable to bending and caused a change in the deflection. The effect was reduced when the bottom of the plate was degraded as well, hence no effect can be seen for composite PULS since symmetric degradation is performed.

The relation between the load and longitudinal end-shortening clarifies the fact that the degradation reduces the stiffness of the plate in the longitudinal direction.

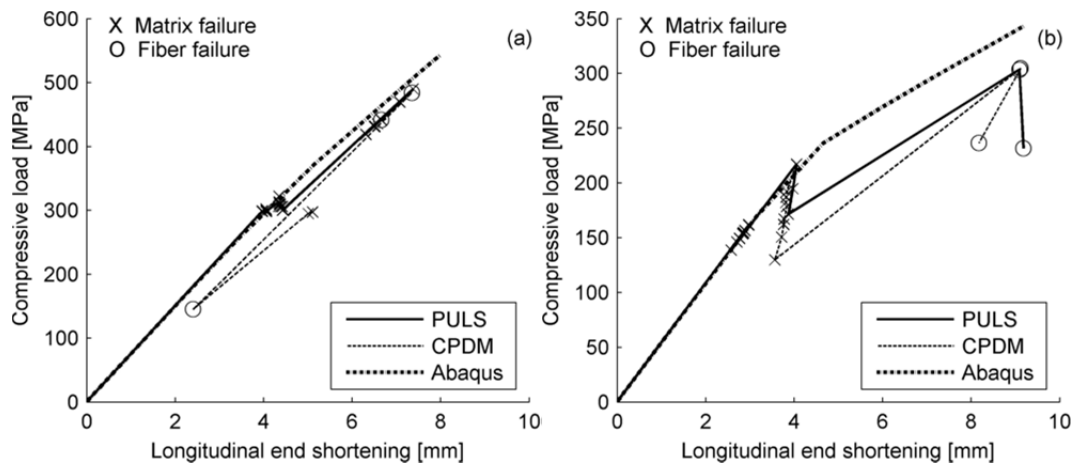


Figure 6.6 Load-longitudinal end-shortening lay-up A $[0_3/+45/90/-45]_{2S}$ (a) and lay-up B $[-45/+45/0]_{4S}$ (b), both with $b/t=10$.

All the calculated ULS results are found in Tables 6.4 and 6.5 and these are compared to Abaqus in a ratio-format in the two columns on the right hand side. The ULS calculated with composite PULS are conservative compared to the calculations performed with Abaqus, and vary between 73% and 94% of the ULS calculated with Abaqus. For the lower b/t -ratios the ULS loads show good agreement with the results obtained with Abaqus, but Figure 6.5 shows that the deflections were greatly under-predicted. This indicates that the bending was of less importance compared to the end shortening, and allowed composite PULS to give a good approximation of the ULS even though shear deformation was not accounted for.

Disregarding shear deformation and the coupling between strain and curvature, bending and twisting, allows for simplifications which reduce calculation time. In Table 6.6, the time of the ULS calculations for composite PULS and CPDM is compared. Composite PULS was expected to have a significantly lower computational time since the coupling terms are disregarded. The degradation model applied in composite PULS should reduce the computational time by half compared to CPDM, since the degradation is symmetrical instead of unsymmetrical. Furthermore, composite PULS expresses the displacements with the deflection, which requires a fewer number of terms. The use of the deflection is believed to contribute to the significant reduction of calculation time.

The simplifications made in composite PULS resulted in a calculation time for the ULS which was only a fraction of the time CPDM used to perform the same task.

Table 6.6 Comparison of computational time for composite PULS and CPDM.

	Lay-up A		Lay-up B	
b/t	PULS	CPDM	PULS	CPDM
10	50s	0h 30min	45s	0h 16min
30	21s	3h 15min	35s	9h 35min
50	30s	4h 28min	28s	23h 50min

6.3 Biaxial load cases

The ULS results from the biaxial load case reflect the results gained from the uniaxial case. Composite PULS is conservative for the plates with higher b/t ratios, but approximate the plates with lower b/t ratios to be too stiff due to Kirchhoff's assumptions. Figures 6.7 and 6.8 present the results for biaxial loading, where both the ULS and eigenvalues for the FE-model and composite PULS are included. First, the results for the plates with high b/t -ratios are discussed and secondly the lower b/t -ratios were investigated for both lay-ups. Due to time limitations only b/t -ratios of 10, 30 and 50 were investigated.

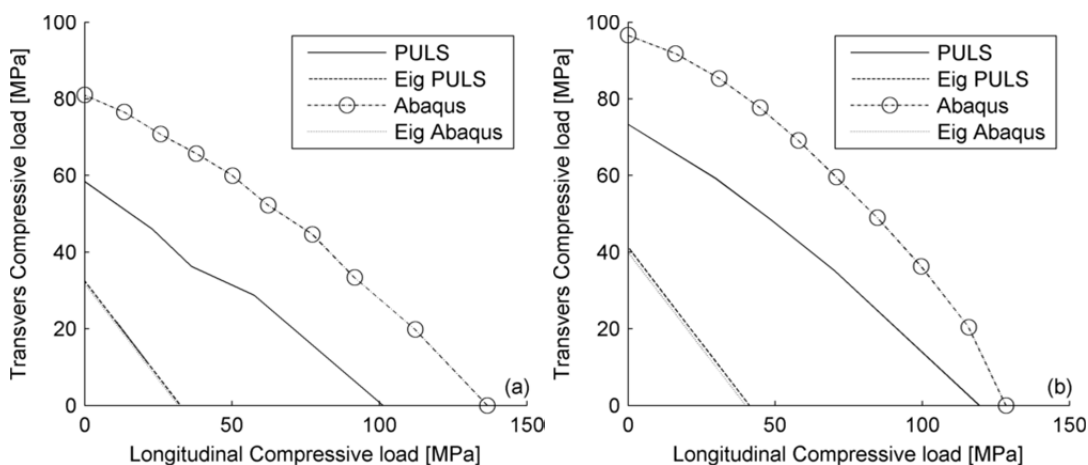


Figure 6.7 Biaxial load case for lay-up A $[0_3/+45/90/-45]_{2S}$ (a) and lay-up B $[-45/+45/0]_{4S}$ (b), both with $b/t=50$.

The calculation of the biaxial case takes approximately twice the time compared to the uniaxial case. This is because the most critical buckling mode has to be evaluated for both the longitudinal and transverse load before calculating the ULS.

For the plates with the highest b/t -ratio the results from the ULS calculation are conservative due to the symmetric complete ply degradation and that the plates are thin, meaning that CLPT is applicable. The eigenvalue for composite PULS and Abaqus closely matched each other and the small difference that was detected was due to the disregarded bending- twisting stiffness terms and the disregarded shear deformation.

The ULS results from the somewhat thicker plates, $b/t=30$, have a similar accuracy compared to the ULS results gained from the $b/t=50$ plates. However, a larger difference for the eigenvalues was observed. The eigenvalues from composite PULS were higher than the ones from Abaqus, caused by the increased out-of-plane shear deformation. For the thickest plates, $b/t=10$, the difference in eigenvalues was clearly observed, see Figure 6.8.

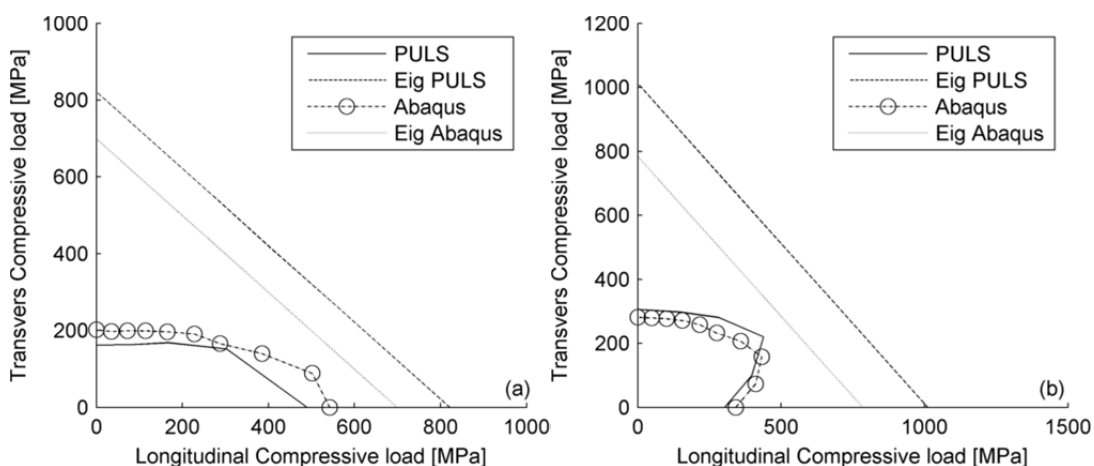


Figure 6.8 Biaxial load case for lay-up A $[0_3/+45/90/-45]_{2S}$ (a) and lay-up B $[-45/+45/0]_{4S}$ (b), both with $b/t=10$.

The reason for similar eigenvalues on both load axes is that the plates are square and that the critical buckling load occurs when the number of half sine waves for both longitudinal and transverse directions is equal to one.

The ULS calculations of the plates with the lowest b/t -ratio show non-conservative values for lay-up B. There could be multiple reasons for the non-conservative answers, where the neglected of out-of-plane shear deformation is considered to be of most significance. The effect of disregarding D_{16} and D_{26} is higher for lay-up B than for lay-up A, since the ratio between D_{16} and D_{11} is higher for lay-up B.

6.4 Delamination

Delamination as a failure mode was not considered in this thesis, since out-of-plane stress contributions were not calculated. The effect of not considering this mode was difficult to predict because it is not known whether delamination was present or not. If delamination was to be present, the results would have been found non-conservative.

In Section 2.3.1, a typical stress-based failure criterion for delamination was presented, which consisted exclusively of out-of-plane stress contributions. For thin plates, these stress contributions were considered to be small. On the other hand, plates with a low b/t ratio were expected to have a larger impact on the out-of-plane stress contributions. It is not known to the authors if this impact would have been large enough to cause delamination without any impact of foreign objects. It should be noted that even though the matrices' material was degraded, the assumption of perfect bonding between layers was never degraded. After a total matrix failure this assumption can seem unrealistic since the matrix-material keeps the laminate intact.

7 Conclusions

The objective of this thesis was to extend PULS so that it can be used for calculating the ULS of single-skin, unstiffened FRP-panels under compressive loads. This was achieved under the following assumptions:

- Kirchhoff's criteria are valid.
- Failure of FRP is well predicted by Hashin-Rotem's criteria.
- No delamination occurs in the laminate.
- The theory for specially orthotropic plates can approximate ULS for general FRP-plates.
- Instantaneous material degradation can be considered in the whole ply after failure.

The ULS was defined as the maximum load-carrying capacity. Compared to the FEA, which included out-of-plane shear but not delamination failure, composite PULS generates reasonable and conservative ULS-estimates for plates with the tested b/t ratios. As the panels' b/t -ratio decreases, the accuracy of the out-of-plane displacement estimates drops resulting in a stiffer response of the plates than received from the FEA, although the ULS estimation is still conservative. A comparison was also made to CPDM, which is based on FSDT, and the curve-fit was found much similar to composite PULS. This indicates that applying CLPT instead of FSDT has a small effect on the ULS estimates with the applied failure criteria.

CLPT does not allow out-of-plane shear, and hence a delamination failure criterion was not included in composite PULS. Disregarding this failure mode can lead to over-predicted results. Another source for over-predicted results is that composite PULS is based on theory especially for orthotropic plates, meaning that D_{16} and D_{26} are zero. However, the effect of this was shown to be small for the parametric study where a comparison of eigenvalues calculated with Abaqus and composite PULS was performed.

When failure is reached, composite PULS degrades the failed material instantaneously, which reduces the stiffness of the material for the whole ply. It was shown that the degradation method is conservative. However the perturbation method cannot handle the stiffness change and therefore the calculation has to restart from zero after each degradation. This is time consuming since there often occurs degradation in each ply before total failure. Furthermore, the computational demand was increased compared to steel because the stress needs to be checked in each ply, which is not the case for steel. The calculation time for composite PULS, given the study cases found in this thesis, varies from half a minute for the simplest case up to one minute for the more complex calculations. Comparison of the calculation time for composite PULS and CPDM showed that composite PULS is significantly faster than CPDM.

Both composite PULS and CPDM contribute to a simplified way of estimating the ULS compared to FEA. Composite PULS has more limiting assumptions compared to the CPDM, although these have little effect on the calculated ULS and the

calculations are performed significantly faster. The work in this thesis has developed a tool that estimates the ULS of composite plates. The estimation of the ULS is less conservative compared to traditional standard methods and faster compared to FEA. A further development of composite PULS could eventually allow for more sustainable designs compared to designs based on methods that today are considered over-conservative.

8 Recommendations for future work

Composite PULS should be investigated for additional lay-ups and material configurations in order to get a deeper understanding of the limitations. For example, a laminate made of materials with a higher longitudinal-transverse stiffness-ratio, E_L/E_T , may introduce possibilities of a different degradation pattern, where perhaps the matrix strength can be disregarded. The possibilities regarding a different degradation pattern should be further investigated, since it is time-consuming to iterate the solution procedure for each degradation. For material where the matrix has a minor contribution to the material strength it can be sufficient to only check first fibre failure without matrix degradation.

There are different opportunities regarding progressive damage models. Composite PULS reloads from zero after each instantaneous degradation, which requires a certain amount of computational time. The possibility to use a linear degradation model instead of an instantaneous degradation model should be investigated. A linear model is generally more time-consuming compared to a model applying instantaneous degradation, but time could be saved when reloading from zero as each degradation is unnecessary. Furthermore, a linear degradation would contribute to a less conservative ULS compared to the instantaneous degradation models.

The laminate is degraded symmetrically due to the disregarded **B**-matrix and the effect of non-symmetric degradation, despite a **B**-matrix equal to zero, should be investigated further in order to see if the degradation can be made less conservative. Another extension that could be added to PULS is to include the coupling between bending and twisting. Including this coupling would mean a higher computational cost but also higher confidence in the result of the ULS calculations. An alternative could be to calculate the ratio between the D_{11} and D_{16} , which would give more awareness of the possible deviation.

To further increase the confidence in the results, the possibility of implementing the FSDT into composite PULS should be evaluated. Since this implementation introduces coupling terms, there could be a high calculation cost.

A reduction of computational cost should be further investigated. One way of achieving less computational cost could be to limit the stress calculations to areas where failure is most likely to occur.

9 References

Agarwal D. Bhagwan, Broutman J. Lawrence, Chandrashekhara K. (2006): *Analysis and performance of fiber composites*, third edition, John Wiley & Sons, Inc, New Jersey.

Ashton J. E. (1969): An Analogy for Certain Anisotropic Plates, *Journal of Composite Materials*, Vol. 3, {April} 1969, pp. 355-358.

Brødrene AA (2013): <http://braa.no/Default.aspx?tabid=8932&language=nb-NO> [Cited, May 11, 2013].

Byklum Eirik (2002): Ultimate strength analysis of stiffened steel and aluminium panels using semi-analytical methods, *Department of Marine Technology*, Norwegian University of Science and Technology, Trondheim, Norway.

Chia Chuen-Yuan (1980): *Nonlinear analysis of plates*, McGraw-Hill, Inc, USA.

Cook R., Malkusw D., Plesha M., Witt R. (2002): *Concepts and Applications of Finite Element Analysis, fourth edition*, John Wiley & sons Inc, Hoboken, USA.

Cui Hai-Po, Wen Wei-Dong, Cui Hai-Tao (2009): An integrated method for predicting damage and residual tensile strength of composite laminates under low velocity impact, *Computers and Structures* 87 (2009), pp 456-466.

Dassault Systèmes [Abaqus]: (2012) Abaqus version 6.12 documentation. Analysis user's manual. Vélizy Villacoublay, France: Dassault Systèmes.

Degenhardt R., Rolfes R., Zimmermann R., Rohwer K. (2006): COCOMAT-improved material exploitation of composite airframe structures by accurate simulation of postbuckling and collapse, *Composite structures* 73, 2006, pp 175-178.

Deuschle H. Matthias, Puck A. (2013): Application of the Puck failure theory for fibre-reinforced composites under three-dimensional stress: Comparison with experimental results, *Journal of Composites Materials*, 2013, 47: 827.

DNV (2013 a): Hull Structural Design, Fibre Composite and Sandwich Constructions, *High Speed, Light Craft and Naval Surface Craft*, Part 3, Chapter 4.

DNV (2013 b):

<http://www.dnv.com/services/software/products/nauticus/hull/bucklingassessment.asp> [Cited, April 25, 2013].

Garnich Mark R., Akula Venkata M. K. (2009): Review of Degradation Models for Progressive Failure Analysis of Fiber Reinforced Polymer Composites, *Applied Mechanics Reviews*, Vol. 62, January 2009.

Hashin Z. (1980): Failure Criteria for Unidirectional Fiber Composites. *Journal of Applied Mechanics*, 47(2), pp 329-334.

Hashin Z., Rotem A. (1973): A Fatigue Failure Criterion for Fiber Reinforced Materials. *Journal of Composite Materials*, Vol. 7, pp 448-464.

Hayman B., Berggreen C., Lundsgaard-Larsen C., Delarche A., Toftegaard H., Dow R. S., Downes J., Misirlis K., Tsouvalis N., Douka C. (2011): Studies of the buckling of composite plates in compression. *Ships and Offshore Structures*, Vol. 6, pp 81-92.

Hinton M. J., Kaddour A. S., Soden P. D. (2002): A comparison of the predictive capabilities of current failure theories for composite laminates, judged against experimental evidence, *Composite Science and Technology*, 62 (2002), pp 1725-1797.

Hollaway L. C., Head P. R. (2001): *Advanced Polymer Composites and Polymers in the Civil Infrastructure*, Elsevier Science Ltd., Oxford, UK, 2001, Ch 4, pp 89-106.

Hu Zhi-gang, Zhang Yan (2010): Continuum damage mechanics based modeling progressive failure of woven-fabric composite laminate under low velocity impact, *Journal of Zhejiang University-Science A (Applied Physics & Engineering)*, 2010 11(3).

IMO (2013):

<http://www.imo.org/KnowledgeCentre/ShipsAndShippingFactsAndFigures/TheRoleandImportanceofInternationalShipping/Documents/International%20Shipping%20-%20Facts%20and%20Figures.pdf>. [Cited, March 14, 2013].

Jonas M. Robert (1999), *Mechanics of Composite Materials*, Second Edition, Taylor & Francis Ltd, London, UK.

Kageyama K., Kimpara I. (1991): Delamination failures in polymer composites, *Material Science and Engineering*, A143(1991), pp 167-174.

Kockums (2013): <http://www.kockums.se/produkter-tjanster/marina-ytfartyg/ytstridsfartyg/korvett-typ-visby/>. [Cited, March 14, 2013].

Krajcinovic D. (1989): Damage Mechanics, *Mechanics of Materials 8*, Aerospace Engineering Department, Arizona, USA, pp 117-197.

LIWEM (2012):

http://liwem.org/en/Documents/LIWEM_2012_presentations_uppdaterad%20aug%202012_del1.pdf [Cited, March 18, 2013].

Maimi P., Camanho P. P., Mayugo J. A., Dávila C. G. (2007): A Continuum damage model for composite laminates: part I – constitutive model, *Mech Mater*, 39(10)(2007,) pp 897-908.

Michaeli W., Mannigel M., Preller F. (2008): On the effect of shear stresses on the fibre failure in CFRP, *Composites Science and Technology*, 69 (2009), pp 1354-1357.

Misirlis K. (2012): *Progressive Collapse Analysis of Composite Ship Hull Sections*. Ph.D. Thesis. School of Marine Science and Technology, Faculty of Science, Agriculture and Engineering, Newcastle University, Newcastle upon Tyne, United Kingdom.

Naval-technology (2013): <http://www.naval-technology.com/projects/dd21/>. [Cited, March 14, 2013].

Reddy J. N. (2004): *Mechanics of Laminated Composite Plates and Shells Theory and Analysis*, second Edition, CRC Press, LLC, Boca Raton.

Reddy J. N. (2007): *Theory and Analysis of Elastic Plates and Shells*, second Edition, Taylor and Francis Group, LLC, Boca Raton.

RINA (2013): http://www.rina.org.uk/composites_in_ships.html. [Cited, March 14, 2013].

Steen E. (1998): Application of the perturbation method to plate buckling problem. *Research Report in Mechanics, No. 98-1, Mechanics Division, Dept. of Mathematics*, University of Oslo, Norway.

Tsai S. W., Wu E. M. (1971): A General Theory of Strength for Anisotropic Materials. *Journal of Composite Materials*, 5, pp 58-80.

Turvey G. J., Marshall I. H. (1995): *Buckling and Postbuckling of Composite Plates*, Chapman and Hall, London, UK.

Yang Q. J. (2013): Post-Buckling and Ultimate Strength Prediction of Composite Plates using a Semi-Analytical Method. *Research Report in Mechanics, No. 1, Mechanics Division, Dept. of Mathematics*, University of Oslo, Norway.

Yang Q. J., Hayman B., Osnes H. (2012): Trials with a Simplified Method for Buckling and Ultimate Strength Analysis of Composite Plates. *Research Report in Mechanics, No. 1, Mechanics Division, Dept. of Mathematics*, University of Oslo, Norway.

Ye L. (1988): Role of matrix resin in delamination onset and growth in composite laminates. *Composite Science and Technology*, Volume 33, Issue 4, pp 257-277.

Appendix A. Classical laminated plate theory

In Appendix A, Classical laminated plate theory presented in Reddy (2004) and Agarwal et al. (2006) is summarized. All equations presented and more elaborated descriptions of the theory are found there.

Laminates consist of several laminae that are assumed to have an infinitesimal thin perfect bond that does not deform from shear, and thus no slippage between laminae. Each lamina may have different directional properties which gives a variation in stress over the thickness of the laminate, even when equally strained.

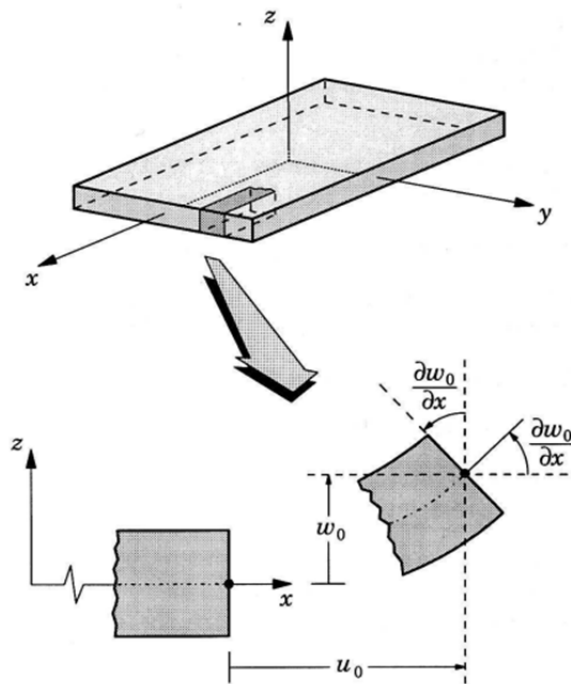


Figure A.1 Undeformed and deformed plate geometry when Kirchhoff's assumptions hold. (Reddy 2004).

CLPT is based on the fact that Kirchhoff's assumptions hold, which are;

- Straight lines perpendicular to the mid-plane (transverse normals) remain straight as the plane deforms into a surface.
- Transverse normals do not experience elongation.
- The transverse normals rotate in such a way that they remain perpendicular to the mid-surface after deformation.

Kirchhoff's assumptions are for a general plate, not specifically a composite plate, and therefore some additional assumptions and restrictions need to be stated:

- The layers are perfectly bonded together.
- The material of each layer is linearly elastic and has three planes of symmetry (orthotropic).

- Each layer is of uniform thickness.
- The strains and displacements are small.
- The transverse shear stress on the top and bottom surface of the laminate is zero.

Given the Cartesian coordinate system with a rectangular plate where the sides are in the x and y axis, *respectively*, and the z axis in the direction of the plate thickness. The Kirchhoff assumptions lead to the following expression:

$$\begin{aligned} u(x, y, z) &= u_0(x, y) - z \frac{\partial w_0}{\partial x}, & w(x, y, z) &= w_0(x, y) \\ v(x, y, z) &= v_0(x, y) - z \frac{\partial w_0}{\partial y} \end{aligned} \quad [\text{mm}] \quad (\text{A.1})$$

Where u, v and w are the displacements in the x, y and z directions at some point in the plate. Furthermore, u_0 and v_0 are the in-plane displacement at a point mid-plane of the plate. It is Important that u_0, v_0 and w_0 are only dependent on x and y . Using the strain-displacement relation the strain is evaluated to

$$\varepsilon_x = \frac{\partial u}{\partial x} + \frac{1}{2} \left(\frac{\partial w}{\partial x} \right)^2, \quad \varepsilon_y = \frac{\partial v}{\partial y} + \frac{1}{2} \left(\frac{\partial w}{\partial y} \right)^2, \quad \gamma_{xy} = \frac{\partial v}{\partial x} + \frac{\partial u}{\partial y} + \frac{\partial w}{\partial x} \frac{\partial w}{\partial y} \quad [-] \quad (\text{A.2})$$

The parameters $\varepsilon_x, \varepsilon_y$ and γ_{xy} are the in-plane normal strain and the in-plane shear strain. Eq (A.1) and (A.2) give

$$\begin{Bmatrix} \varepsilon_x \\ \varepsilon_y \\ \gamma_{xy} \end{Bmatrix} = \begin{Bmatrix} \varepsilon_x^0 \\ \varepsilon_y^0 \\ \gamma_{xy}^0 \end{Bmatrix} + z \begin{Bmatrix} k_x \\ k_y \\ k_{xy} \end{Bmatrix} = \begin{Bmatrix} \frac{\partial u^0}{\partial x} + \frac{1}{2} \left(\frac{\partial w_0}{\partial x} \right)^2 \\ \frac{\partial v^0}{\partial y} + \frac{1}{2} \left(\frac{\partial w_0}{\partial y} \right)^2 \\ \frac{\partial v^0}{\partial x} + \frac{\partial u^0}{\partial y} + \frac{\partial w_0}{\partial x} \frac{\partial w_0}{\partial y} \end{Bmatrix} + z \begin{Bmatrix} -\frac{\partial^2 w}{\partial x^2} \\ -\frac{\partial^2 w}{\partial y^2} \\ -2 \frac{\partial^2 w}{\partial x \partial y} \end{Bmatrix} \quad [-] \quad (\text{A.3})$$

Where k_x, k_y and k_{xy} are the curvature of the plate and ε^0 is the membrane-strain. The combined Equation (A.3) with the stress-strain relationship in E.3 gives

$$\{\sigma\}_k = [\bar{\mathbf{Q}}]_k \{\varepsilon^0 + z\mathbf{k}\} \quad [\text{MPa}] \quad (\text{A.4})$$

Where k represents the layer number in the laminate. Note that it is only the strain in the mid-plane and the curvature that are functions of x and y . Furthermore, the $[\bar{\mathbf{Q}}]_k$ -matrix is constant across the thickness of each lamina, which will generate a stress “jump” between laminas since the stiffness of the laminate changes over the infinitesimal bond between the layers.

Due to the fact that the stresses vary between the layers, it is common to calculate the responses from the resultant force and moment acting on a laminate cross section instead of explicitly expressing the response due to the stresses. The forces are defined by integrating the stresses over the laminate thickness:

$$\begin{aligned} N_x &= \int_{-h/2}^{h/2} \sigma_x dz \\ N_y &= \int_{-h/2}^{h/2} \sigma_y dz \quad [\text{N/mm}] \\ N_{xy} &= \int_{-h/2}^{h/2} \sigma_{xy} dz \end{aligned} \quad (\text{A.5})$$

Likewise, the moment responses are defined by integrating the stress over the thickness and multiply with the moment arm:

$$\begin{aligned} M_x &= \int_{-h/2}^{h/2} \sigma_x z dz \\ M_y &= \int_{-h/2}^{h/2} \sigma_y z dz \quad [\text{N}] \\ M_{xy} &= \int_{-h/2}^{h/2} \sigma_{xy} z dz \end{aligned} \quad (\text{A.6})$$

The positive sense of orientation of the responses follows the stress convention defined in Agarwal et al. (2006). By converting the stresses to force-responses and moment-responses, the system is reduced so as not to contain laminate thickness or z coordinate explicitly. Consider a setup of n orthotropic lamina with various thicknesses stacked in a laminate. Here the force-responses and moment-responses over the mid-plane could be replaced with a stepwise integral over each lamina.

$$\{\mathbf{N}\} = \int_{-h/2}^{h/2} \{\boldsymbol{\sigma}\} dz = \sum_{k=1}^n \int_{h_{k-1}}^{h_k} \{\boldsymbol{\sigma}\}_k dz \quad [\text{N/mm}] \quad (\text{A.7})$$

$$\{\mathbf{M}\} = \int_{-h/2}^{h/2} \{\boldsymbol{\sigma}\} z dz = \sum_{k=1}^n \int_{h_{k-1}}^{h_k} \{\boldsymbol{\sigma}\}_k z dz \quad [\text{N}] \quad (\text{A.8})$$

Equations (A.7) and (A.8) may be expressed with the use of a membrane strain and curvature in (A.4).

$$\{\mathbf{N}\} = \sum_{k=1}^n \int_{h_{k-1}}^{h_k} [\bar{\mathbf{Q}}]_k \{\boldsymbol{\varepsilon}^0\} dz + \int_{h_{k-1}}^{h_k} [\bar{\mathbf{Q}}]_k \{\mathbf{k}\} z dz \quad [\text{N/mm}] \quad (\text{A.9})$$

$$\{\mathbf{M}\} = \sum_{k=1}^n \int_{h_{k-1}}^{h_k} [\bar{\mathbf{Q}}]_k \{\boldsymbol{\varepsilon}^0\} z dz + \int_{h_{k-1}}^{h_k} [\bar{\mathbf{Q}}]_k \{\mathbf{k}\} z^2 dz \quad [\text{N}] \quad (\text{A.10})$$

After further investigation of Equations (A.9) and (A.10) it is noted that the mid-plane strains, curvatures and the stiffness matrix are constant within each layer, and hence could be moved out of the integral. The result is that the force and moment response expression could be simplified into

$$\{\mathbf{N}\} = \sum_{k=1}^n [\bar{\mathbf{Q}}]_k \int_{h_{k-1}}^{h_k} dz \{\boldsymbol{\varepsilon}^0\} + [\bar{\mathbf{Q}}]_k \int_{h_{k-1}}^{h_k} z dz \{\mathbf{k}\} \quad [\text{N/mm}] \quad (\text{A.11})$$

$$\{\mathbf{M}\} = \sum_{k=1}^n [\bar{\mathbf{Q}}]_k \int_{h_{k-1}}^{h_k} z dz \{\boldsymbol{\varepsilon}^0\} + [\bar{\mathbf{Q}}]_k \int_{h_{k-1}}^{h_k} z^2 dz \{\mathbf{k}\} \quad [\text{N}] \quad (\text{A.12})$$

Recognizing the coupling between the force and the moment response the expression could be summarized into

$$\begin{Bmatrix} \mathbf{N} \\ \mathbf{M} \end{Bmatrix} = \begin{bmatrix} \mathbf{A} & \mathbf{B} \\ \mathbf{B} & \mathbf{D} \end{bmatrix} \begin{Bmatrix} \boldsymbol{\varepsilon}^0 \\ \mathbf{k} \end{Bmatrix} \quad \begin{matrix} [\text{N/mm}] \\ [\text{N}] \end{matrix} \quad (\text{A.13})$$

Where \mathbf{A} , \mathbf{B} and \mathbf{D} -matrices are called *extensional stiffness matrix*, *coupling matrix* and *bending matrix*. They are formulated using the stiffness matrix for the lamina and the thickness of each lamina according to:

$$\begin{aligned} A_{ij} &= \sum_{k=1}^n \bar{Q}_{ij} (h_k - h_{k-1}) \quad [\text{N/mm}] \\ B_{ij} &= \sum_{k=1}^n \bar{Q}_{ij} (h_k^2 - h_{k-1}^2) \quad [\text{N}] \\ D_{ij} &= \sum_{k=1}^n \bar{Q}_{ij} (h_k^3 - h_{k-1}^3) \quad [\text{Nmm}] \end{aligned} \quad (\text{A.14})$$

The bending matrix is a coupling matrix between bending and extension of the lamina, meaning that an extension will cause bending or vice versa. Since the stiffness matrix is only dependent on the lay-up angle, if the material is the same through the laminate, symmetry is often used. In the symmetry case, the thickness terms cancel out each other and the coupling matrix becomes zero.

Appendix B. First-order shear deformation theory (FSDT)

In Appendix B, the first-order shear deformation theory presented in Reddy (2004) and Agarwal et al. (2006) is summarized. All equations presented and more elaborated descriptions of the theory may be found in these works.

FSDT is a relaxation of Kirchhoff's assumption where the transverse normals must be straight, but not necessarily perpendicular to the mid-surface, see Figure B.1.

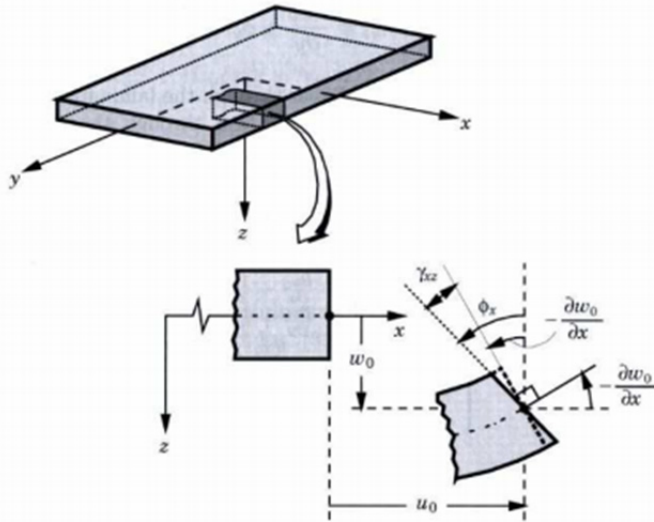


Figure B.1 Undeformed and deformed geometries of a plate under the assumptions of the first-order plate theory, Reddy (2004).

The relaxed assumption results in that the displacement field is somewhat modified to:

$$\begin{aligned} u(x, y, z) &= u_0(x, y) - z\phi_x(x, y) & v(x, y, z) &= v_0(x, y) - z\phi_y(x, y), \\ w(x, y, z) &= w_0(x, y), \end{aligned} \quad [\text{mm}] \quad (\text{B.1})$$

where u, v and w are the displacements in the x, y and z directions at some point in the plate, and ϕ_x and ϕ_y indicate the rotations of a transverse normal about the x and y axis, respectively, and can be expressed as:

$$\phi_x = \frac{\partial u}{\partial z}, \quad \phi_y = \frac{\partial v}{\partial z} \quad [-] \quad (\text{B.2})$$

The same steps as for CLPT can be followed in order to calculate the stiffness matrices. However the shear contribution needs to be accounted for. It is convenient to split the strains into two parts, one bending part, ε_b , and one shearing part, ε_s .

$$\boldsymbol{\varepsilon}_b = \begin{Bmatrix} \varepsilon_x \\ \varepsilon_y \\ \gamma_{xy} \end{Bmatrix} = \begin{Bmatrix} \frac{\partial u^0}{\partial x} + \frac{1}{2} \left(\frac{\partial w_0}{\partial x} \right)^2 \\ \frac{\partial v^0}{\partial y} + \frac{1}{2} \left(\frac{\partial w_0}{\partial y} \right)^2 \\ \frac{\partial v^0}{\partial x} + \frac{\partial u^0}{\partial y} + \frac{\partial w_0}{\partial x} \frac{\partial w_0}{\partial y} \end{Bmatrix} + z \begin{Bmatrix} \frac{\partial \phi_x}{\partial x} \\ \frac{\partial \phi_y}{\partial y} \\ \frac{\partial \phi_x}{\partial y} + \frac{\partial \phi_y}{\partial x} \end{Bmatrix} \quad [-] \quad (\text{B.3})$$

$$\boldsymbol{\varepsilon}_s = \begin{Bmatrix} \gamma_{yz} \\ \gamma_{xz} \end{Bmatrix} = \begin{Bmatrix} \phi_y + \frac{\partial w_0}{\partial y} \\ \phi_x + \frac{\partial w_0}{\partial x} \end{Bmatrix} \quad [-] \quad (\text{B.4})$$

Since the transverse shear strains are assumed to be constant through the laminate thickness, the stresses must be constant as well. It is known that the shear is not constant but rather square for composite plates (Reddy 2004), although this is compensated for with a parameter K , called the *shear correction factor*. The relation between shear strain and shear force is expressed as:

$$\begin{Bmatrix} R_{yz} \\ R_{xz} \end{Bmatrix} = \begin{bmatrix} A_{44} & A_{45} \\ A_{45} & A_{55} \end{bmatrix} \begin{Bmatrix} \gamma_{yz} \\ \gamma_{xz} \end{Bmatrix} \quad [\text{N/mm}] \quad (\text{B.5})$$

Where

$$A_{ji} = K \int_{-h/2}^{h/2} \bar{Q}_{ji} dz \quad [\text{N/mm}] \quad (\text{B.6})$$

\bar{Q}_{ji} is the transformed stiffness coefficient, and a value of 5/6 is commonly used for K . The added shear contribution will couple the displacement fields even for the simplest of special cases, especially an orthotropic lay-up.

Appendix C. Energy principles

In this appendix, different energy principles applied in the thesis are summarized. Further descriptions are found in Reddy (2004), Reddy (2007) and Byklum (2002)

Potential energy

The potential energy of a system describes the energy within the system, which is the same as specifying the amount of work that the system can perform. The potential energy consists of internal/elastic strain energy and the potential of applied loads. The potential of applied loads is related to the work done by the force during displacement in the system.

When no accelerations are present in the system, the potential energy is:

$$\Pi = U + V \text{ [Nmm]} \quad (\text{C.1})$$

Where U is the internal strain energy and V is the external load potential.

An investigation of the concept *strain energy* per unit volume, also known as *energy strain density*, describes the energy needed to deform one volume unit and is denoted U_0 .

$$U_0 = \int_{\boldsymbol{\varepsilon}} \boldsymbol{\sigma}^T d\boldsymbol{\varepsilon} = \frac{1}{2} \boldsymbol{\sigma}^T \boldsymbol{\varepsilon} = \frac{1}{2} \boldsymbol{\varepsilon}^T \mathbf{E} \boldsymbol{\varepsilon} \text{ [Nmm]} \quad (\text{C.2})$$

The total energy strain energy is then the integration of the strain energy density over the volume of the body.

$$U = \int_v U_0 dv = \frac{1}{2} \int_v \boldsymbol{\varepsilon}^T \mathbf{E} \boldsymbol{\varepsilon} dv \text{ [Nmm]} \quad (\text{C.3})$$

Equations (C.2) and (C.3) are both general when all six strains and stresses are regarded and the material matrix, \mathbf{E} , is six by six. If Kirchhoff's thin plate theory is adopted the system is reduced to a three by three, since the strain in the transverse directions are disregarded. However, using the relaxed Kirchhoff's assumption (first-order shear deformation) the shear strains need to be accounted for and reduce the stress and strain vectors to five and the material matrix to a five by five. The strain energy of the system can be divided into membrane-energy and bending-energy, U_p , and shearing-energy, U_s , partly breaking down the problem.

The external load potential, V , consists of body forces, \mathbf{f} , per unit volume and surface tractions, \mathbf{t} , per unit area of the boundary, S .

$$V = -\left(\int_v \mathbf{u}^T \mathbf{f} dv + \int_S \mathbf{u}^T \mathbf{f} ds \right) \text{ [Nmm]} \quad (\text{C.4})$$

\mathbf{u} is the displacement and the negative sign indicates that the work is done on the body. The body forces are integrated over the volume for infinitesimal elements, while the surface forces are integrated over the surface. With Equations (C.3) and (C.4) in (C.1) an expression for the total potential energy is obtained.

$$\Pi = U + V = \frac{1}{2} \int_v \boldsymbol{\varepsilon}^T \mathbf{E} \boldsymbol{\varepsilon} dv - \left(\int_v \mathbf{u}^T \mathbf{f} dv + \int_s \mathbf{u}^T \mathbf{f} ds \right) \text{ [Nmm]} \quad (\text{C.5})$$

Virtual work principles

The principle of virtual work is that a static equilibrium is achieved when the sum of the work done by the internal and external forces are zero for all virtual deformations and strains. Virtual deformations are imagined to take place via a mechanical system that is made out of admissible functions. The functions that fulfil the geometric constraints, not necessarily Newton's second law, will yield more accurate results. These deformations do not need to have any relation to the actual displacement caused by the loading (Reddy 2004).

$$\delta U + \delta V = 0 \text{ [Nmm]} \quad (\text{C.6})$$

The delta symbol δ is the *variational operator*, used for denoting the variation (change) of the internal virtual work, U , and the external virtual work, V , in the plate. The virtual work is found by using the variational operator on the potential energy expressions, introduced in Section Potential energy, which gives a model that is very general and could be implemented on non-conservative solutions. Since the calculations performed and evaluated in this thesis are done by incremental methods, the rate relative to the parameter of interest for each step is evaluated giving (C.7).

$$\delta \dot{U} + \delta \dot{V} = 0 \text{ [Nmm]} \quad (\text{C.7})$$

The dot represents the differentiation with regard to the rate parameter.

The principle of minimum potential energy

Derived straight from the principle of virtual work, the principle of minimum potential energy is: all the possible deflections satisfying kinematic compatibility, those which satisfy static equilibrium, will give a stationary value of the potential energy of the body:

$$\delta \Pi = \delta U + \delta V = 0 \text{ [Nmm]} \quad (\text{C.8})$$

The principle allows for non-elastic materials. However, the system needs to be conservative or reversible in order for the principle to be established.

It can be shown that the stationary value of the total potential energy is a minimum value. Given that the potential energy in the system can be described by independent variables x_n the minimum must be obtained for each of these. The principle can also be used on rate form, where the unit depends on the unit of x_n .

$$\frac{\partial \Pi}{\partial x_n} = 0 \text{ [Nmm]} \text{ and } \left(\frac{\partial \dot{\Pi}}{\partial x_n} \right) = 0 \quad (\text{C.9})$$

Appendix D. Rayleigh-Ritz method

Appendix D presents the Rayleigh-Ritz method. For a further description, see Cook et al. (2002), Turvey et al. (1995) and Byklum (2002)

The Rayleigh-Ritz method is a classic approximation method of eigenvalue problems, most of all used on the vibration problem of plates. The method, which Walter Ritz evolved from Lord Rayleigh's method for approximation of natural frequencies for single-degree of freedom (SDOF) systems in the early 20th century, is applicable on buckling and postbuckling problems as well. The expansion takes the Rayleigh SDOF solution to multiple DOF by introducing a series of approximating functions in order to solve eigenvalue problems, Cook et al. (2002).

The Rayleigh-Ritz method consists of admissible functions that, together with unknown amplitudes, describe the wanted variable, where the unknown amplitudes are found using the principle of minimum potential energy. The total potential energy of the system is described by the displacement, which means that the potential energy is described by several linear independent functions. Since the total potential energy is a minimum, the differential is zero and this must be true for all linear combinations that explain the potential energy.

$$\Pi = \Pi(a_1, a_2 \dots a_n) \text{ [Nmm]} \quad (\text{D.1})$$

$$\frac{\partial \Pi}{\partial \mathbf{a}} = \frac{\partial \Pi}{\partial a_1} = \frac{\partial \Pi}{\partial a_2} = \dots = \frac{\partial \Pi}{\partial a_n} = 0 \quad (\text{D.2})$$

The functions used in the approximation are called shape or trail functions and are a Fourier's series which, given the sufficient number of terms in the series, express a correct displacement and rotation for the plate. An example of such a set-up can be the description of out-of-plane displacement of a plate.

$$w_l = \sum_{i=1}^l P_i \alpha_i(x_i) \text{ [mm]} \quad (\text{D.3})$$

where w_l is the displacement, P is the amplitude and $\alpha_i(x_i)$ is the admissible functions. When the displacement is put into the potential energy equations there is an equation system with as many unknowns as solutions, and therefore the unknowns can be solved. This could be extended to include all displacements and rotations as well, only increasing the size of the equations system that needs to be solved.

The functions describing the displacement are approximate and the approximation should be investigated. Since the energy is a minimum, the displacement that requires the *least* amount of energy will take place, meaning that unless the exact displacement is guessed it will be demand more energy. In other words, a greater force than demanded for the displacement is calculated. This means that the structure is assumed to be stiffer than it actually is giving a false impression that it can withstand higher loads. Generally this error is reduced as a greater number of terms are increased. However, if the exact displacement function is assumed this is not the case.

All the generalized degrees of freedom can be collected in a vector \mathbf{A} that gives an expression using variational variables in vector form:

$$\frac{\partial \Pi}{\partial \mathbf{A}} \delta \mathbf{A} = \left(\frac{\partial U}{\partial \mathbf{A}} + \frac{\partial V}{\partial \mathbf{A}} \right) \delta \mathbf{A} = 0 \quad (\text{D.9})$$

Appendix E. Composite and buckling theory

Appendix E gives a short introduction of the basic composite theory. For a further description, see Agarwal et al. (2006).

For an orthotropic material, three-dimensioned stress-strain relations require nine independent elastic constants, and for a two-dimensional relation four constants are required. Below is the stress-strain relation for a two-dimensional orthotropic plate;

$$\begin{Bmatrix} \sigma_1 \\ \sigma_2 \\ \tau_{12} \end{Bmatrix} = \begin{bmatrix} Q_{11} & Q_{12} & 0 \\ Q_{21} & Q_{22} & 0 \\ 0 & 0 & Q_{33} \end{bmatrix} \begin{Bmatrix} \varepsilon_1 \\ \varepsilon_2 \\ \gamma_{12} \end{Bmatrix} \text{ [MPa]} \quad (\text{E.1})$$

The simplification made for an orthotropic material is that no shear strain occurs when loaded in normal directions to the lamina orientation. If the lamina orientation is equal to the reference axis it is called specially orthotropic. For a lamina where the longitudinal and the transverse directions are the material coordinate axis ($\sigma_1 = \sigma_L; \sigma_2 = \sigma_T$), the $[\mathbf{Q}]$ -matrix can be evaluated to be

$$\begin{aligned} Q_{11} &= \frac{E_L}{1 - \nu_{LT}\nu_{TL}} \\ Q_{22} &= \frac{E_T}{1 - \nu_{LT}\nu_{TL}} \quad \text{[MPa]} \\ Q_{12} &= \frac{\nu_{TL}E_L}{1 - \nu_{LT}\nu_{TL}} = \frac{\nu_{LT}E_T}{1 - \nu_{LT}\nu_{TL}} \\ Q_{66} &= G_{LT} \end{aligned} \quad (\text{E.2})$$

When laminates are constructed the fibre-orientation relative to a coordinate system becomes important. The stress-strain relation can be transformed into a Cartesian coordinate system using the transformation matrix $[\mathbf{T}_1]$ and $[\mathbf{T}_2]$, see Agarwal et al. (2006), which gives

$$\begin{Bmatrix} \sigma_x \\ \sigma_y \\ \tau_{xy} \end{Bmatrix} = [\mathbf{T}_1]^{-1} \begin{bmatrix} Q_{11} & Q_{12} & 0 \\ Q_{21} & Q_{22} & 0 \\ 0 & 0 & Q_{33} \end{bmatrix} [\mathbf{T}_2] \begin{Bmatrix} \varepsilon_x \\ \varepsilon_y \\ \gamma_{xy} \end{Bmatrix} = \begin{bmatrix} \bar{Q}_{11} & \bar{Q}_{12} & \bar{Q}_{13} \\ \bar{Q}_{21} & \bar{Q}_{22} & \bar{Q}_{23} \\ \bar{Q}_{31} & \bar{Q}_{32} & \bar{Q}_{33} \end{bmatrix} \begin{Bmatrix} \varepsilon_x \\ \varepsilon_y \\ \gamma_{xy} \end{Bmatrix} \text{ [MPa]} \quad (\text{E.3})$$

Thus the $[\bar{\mathbf{Q}}]$ -matrix gives the relation between the stress and strain in a coordinate system with an arbitrary axis to the coordinate system of the lamina.

Appendix F. Complete ply degradation model (CPDM)

In Appendix F, each step of the complete ply degradation model (CPDM) is described in the following order; calculations of displacements, rotations and load parameter, solution method and degradation model. All equations presented in this section are taken from Yang (2013), where a more elaborated description of the model can be found.

Displacement and load parameters

The displacements and rotations for a simply supported plate that is subjected to a uniaxial compression load are calculated using the Rayleigh-Ritz method. The boundary condition is fulfilled using the double Fourier series with the corresponding shape functions, see Yang et al. (2012).

$$u_0(x, y) = \sum_{n=1}^{\infty} \sum_{m=1}^{\infty} u_{mn} \sin\left(\frac{m\pi x}{a}\right) \sin\left(\frac{n\pi y}{b}\right) + u_c \frac{x}{a} \quad [\text{mm}] \quad (\text{F.1})$$

$$v_0(x, y) = \sum_{n=1}^{\infty} \sum_{m=1}^{\infty} v_{mn} \sin\left(\frac{m\pi x}{a}\right) \sin\left(\frac{n\pi y}{b}\right) + v_c \frac{y}{b} \quad [\text{mm}] \quad (\text{F.2})$$

$$\phi_x(x, y) = \sum_{n=1}^{\infty} \sum_{m=1}^{\infty} x_{mn} \cos\left(\frac{m\pi x}{a}\right) \sin\left(\frac{n\pi y}{b}\right) \quad [\text{rad}] \quad (\text{F.3})$$

$$\phi_y(x, y) = \sum_{n=1}^{\infty} \sum_{m=1}^{\infty} y_{mn} \sin\left(\frac{m\pi x}{a}\right) \cos\left(\frac{n\pi y}{b}\right) \quad [\text{rad}] \quad (\text{F.4})$$

$$\begin{aligned} w_{tot}(x, y) &= w(x, y) + w_{ini}(x, y) \\ &= \sum_{n=1}^{\infty} \sum_{m=1}^{\infty} w_{mn} \sin\left(\frac{m\pi x}{a}\right) \sin\left(\frac{n\pi y}{b}\right) + \sum_{n=1}^{\infty} \sum_{m=1}^{\infty} w_{imn} \sin\left(\frac{m\pi x}{a}\right) \sin\left(\frac{n\pi y}{b}\right) \quad [\text{mm}] \end{aligned} \quad (\text{F.5})$$

Here u_0 , v_0 and w_{tot} are the mid-plane strains in the x and y -direction, respectively, and the out-of-plane displacement while ϕ_x and ϕ_y are the rotations around the x and y -axis. The displacement and rotations are expressed with the unknown series amplitudes u_c , u_{mn} , v_c , v_{mn} , x_{mn} , y_{mn} and w_{mn} , while m and n are the positive integers, and w_{mn} the initial imperfection amplitude. These unknowns are for simplicity's sake collected in a variable λ_i .

$$\begin{aligned} [\lambda_i] &= [\lambda_1, \lambda_2, \dots, \lambda_{N_{tot}}] \\ &= [u_c, u_{11}, \dots, u_{NM}, \\ &\quad v_c, v_{1,1}, \dots, v_{NM}, \\ &\quad x_{1,1}, \dots, x_{NM}, \\ &\quad y_{1,1}, \dots, y_{NM}, \\ &\quad w_{1,1}, \dots, w_{NM},] \quad [-] \end{aligned} \quad (\text{F.6})$$

The unknowns are solved using the Rayleigh-Ritz method and incrementally computing the rate of the equilibrium equations with respect to an arc length parameter η . The Rayleigh-Ritz method uses the principles of minimum potential energy in order to calculate the unknown amplitudes. In order to achieve a good overview of the problem, the internal strain energy is divided into; in-plan strain energy and shear strain energy.

$$\Pi = U_p + U_s + V \text{ [Nmm]} \quad (\text{F.7})$$

The in-plane strain is further divided into potential membrane and bending strains and potential strains, respectively, due to the coupling terms between the membrane-strain and bending-strain energy.

$$U_p = U_m + U_b + U_{mb} \text{ [Nmm]} \quad (\text{F.8})$$

The reason for this separation is that the terms are dependent on the separate stiffness matrix; extensional stiffness matrix, bending stiffness matrix and the coupling matrix, in that order. The internal energy is a function of the strains and curvatures. Since the strains and curvatures are non-linear with regard to the out-of-plane deflection in the x and y -direction, these energy terms will be non-linear.

The potential energy due to the external forces in the x -direction is given by:

$$V = \Lambda N_x b u_c \text{ [Nmm]} \quad (\text{F.9})$$

where Λ is a load parameter, b is the width of the plate and u_c is the plate shortening in the x -direction.

With the energy expressions in Appendix C the unknown can be solved. However solving the equation system for non-linear terms is hard. Rather than solving these non-linear equations directly they are solved by using the arc length parameter to incrementally compute the rate of the equilibrium functions, a procedure known as the arc length method, Figure F.1. The application of the method for plate buckling problems and the evaluation of alternative perturbation methods, with regard to large plate deformation theory, has been done by Steen (1998) and is included in CPDM.

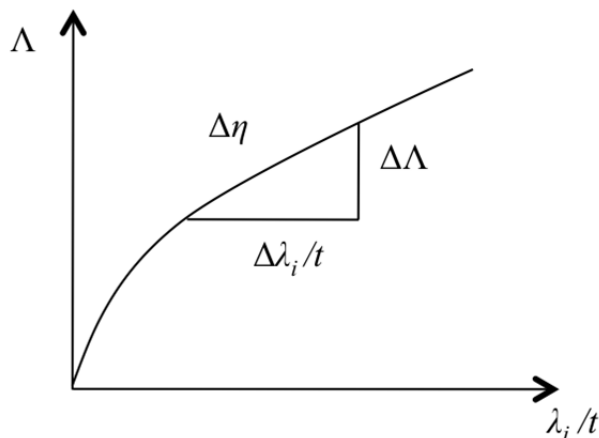


Figure F.1 The arc-length method.

For a small enough arc-length parameter the right-angle triangle shown in Figure F.1 allows the use of the Pythagorean theorem to express the relation between the arc-length parameter, the displacement amplitude above the thickness and the load parameter.

$$\Lambda^2 + \sum_{i=1}^{N_{tot}} \left(\frac{\dot{\lambda}_i}{t} \right)^2 = 1 \quad (\text{F.10})$$

The dot-mark above the symbols indicates that it has been differentiated with respect to the arc length parameter. The importance of a small arc length parameter increment $\Delta\eta$ becomes further apparent when regarding the equilibrium curve from point s to $(s + 1)$ where a Taylor expansion gives

$$\lambda_i^{s+1} = \lambda_i^s + \frac{\dot{\lambda}_i^s}{1!} (\Delta\eta)^1 + \frac{\ddot{\lambda}_i^s}{2!} (\Delta\eta)^2 + \frac{\dddot{\lambda}_i^s}{3!} (\Delta\eta)^3 + \dots \quad (\text{F.11})$$

$$\Lambda^{s+1} = \Lambda^s + \frac{\dot{\Lambda}^s}{1!} (\Delta\eta)^1 + \frac{\ddot{\Lambda}^s}{2!} (\Delta\eta)^2 + \frac{\ddot{\Lambda}^s}{3!} (\Delta\eta)^3 + \dots \quad (\text{F.12})$$

In CPDM only the first two terms of the Taylor expansion, in Equations (F.11) and (F.12), are accounted for, which means that calculated values using a large $\Delta\eta$ will give a load parameter that is higher compared to a small $\Delta\eta$ until convergence is achieved. Considering this increment, the method is found non-conservative since the in-plane stresses for each ply are calculated from the displacement and rotations that, in the model, are lower than the actual displacement and rotations.

In order to solve the unknown amplitudes, the Rayleigh-Ritz method is expressed for each increment with the potential energy given in Equation (D.9).

$$\frac{\partial \Pi}{\partial \lambda_i} = \frac{\partial^2 \Pi}{\partial \lambda_i \partial \lambda_j} \frac{\partial \lambda_j}{\partial \eta} + \frac{\partial^2 \Pi}{\partial \lambda_i \partial \Lambda} \frac{\partial \Lambda}{\partial \eta} = 0 \quad (\text{F.13})$$

The equation consists of N_{tot} equations and $N_{tot} + 1$ unknowns, where the last needed equation is Equation (F.10).

From Equations (F.10) and (F.13) the load rate parameter $\dot{\Lambda}$ can be established:

$$\dot{\Lambda} = \pm \frac{t}{\sqrt{\left(t^2 + \sum_{i,j=1}^{N_{tot}} \left(\left(\frac{\partial^2 \Pi}{\partial \lambda_i \partial \lambda_j} \right)^{-1} \frac{\partial^2 \Pi}{\partial \lambda_i \partial \Lambda} \right)^2 \right)}} \quad (\text{F.14})$$

With the respective displacements found, the in-plane stresses σ_x , σ_y and τ_{xy} can be calculated using the relations described in Appendix A and B. The stresses are calculated in each ply with a 10mm spacing in the x - and y -direction in order to perform a failure check according to Hashin-Rotem's failure criteria.

Failure initiation, material degradation and recalculation of material stiffness

With the stresses calculated, failure initiation is checked according to the Hashin-Rotem's failure criteria, and if none of the failure criteria are violated the load propagation continues until a failure is detected.

When a failure is detected in a ply or several plies, the material needs to be degraded due to a reduced stiffness. CPDM excludes the failed material for the entire ply that has fulfilled the failure criterion. Degradation of the complete ply is conservative, since undamaged material that would contribute to structural stiffness is degraded as well. It is the conservativeness of this degradation process that makes CPDM conservative with respect to traditional FE-calculations.

CPDM reduces the stiffness of the structure instantaneously when failure occurs with a defined damage factor, $d_i = 0.99$. The new stiffness is calculated by reducing the affected material parameters (matrix or/and fibre) depending on the failure. When the stiffness has been recalculated the plate properties have been changed and the iterative process explained in previous sections needs to be restarted from the unloaded case in order to have a known displacement (initial).

Appendix G. Equations used in calculation of the critical energy release rate

Appendix G presents the equations used for calculating the critical energy release rate, corresponding to the area of the large triangle, see Figure G.1, which are used as inputs in Abaqus, see Abaqus (2012).

Fibre tension:

$$\begin{aligned}\delta_{eq}^{ft} &= L^c \sqrt{\langle \varepsilon_{11} \rangle^2 + \alpha \varepsilon_{12}^2} \\ \sigma_{eq}^{ft} &= \frac{\langle \sigma_{11} \rangle \langle \varepsilon_{11} \rangle + \alpha \tau_{12} \varepsilon_{12}}{\delta_{eq}^{ft} / L^c}\end{aligned}\quad (G.1)$$

Fibre compression:

$$\begin{aligned}\delta_{eq}^{fc} &= L^c \langle -\varepsilon_{11} \rangle \\ \sigma_{eq}^{fc} &= \frac{\langle -\sigma_{11} \rangle \langle -\varepsilon_{11} \rangle}{\delta_{eq}^{fc} / L^c}\end{aligned}\quad (G.2)$$

Matrix tension:

$$\begin{aligned}\delta_{eq}^{mt} &= L^c \sqrt{\langle \varepsilon_{22} \rangle^2 + \varepsilon_{12}^2} \\ \sigma_{eq}^{mt} &= \frac{\langle \sigma_{22} \rangle \langle \varepsilon_{22} \rangle + \tau_{12} \varepsilon_{12}}{\delta_{eq}^{mt} / L^c}\end{aligned}\quad (G.3)$$

Matrix compression:

$$\begin{aligned}\delta_{eq}^{mc} &= L^c \sqrt{\langle -\varepsilon_{22} \rangle^2 + \varepsilon_{12}^2} \\ \sigma_{eq}^{mc} &= \frac{\langle -\sigma_{22} \rangle \langle -\varepsilon_{22} \rangle + \tau_{12} \varepsilon_{12}}{\delta_{eq}^{mc} / L^c}\end{aligned}\quad (G.4)$$

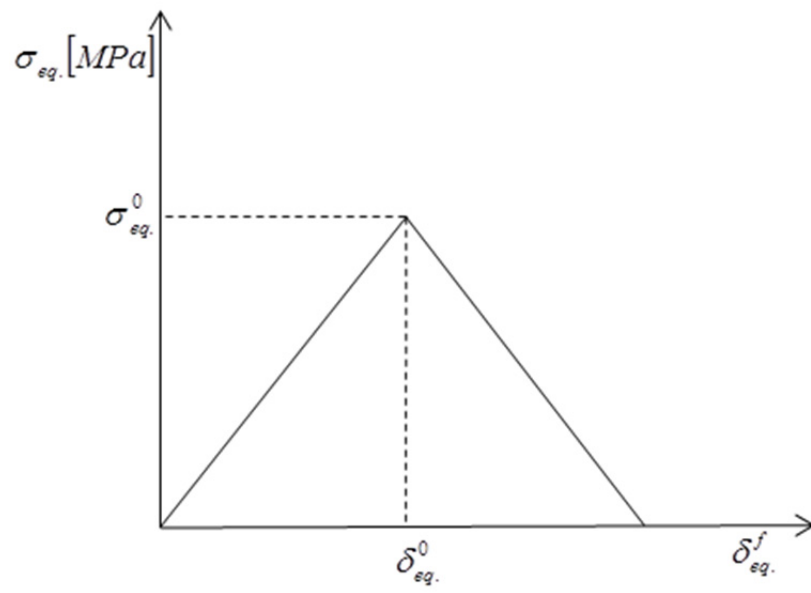


Figure G.1 Equivalent stress –and displacement relation for damage evolution.

Appendix H. Results of the mesh convergence study Abaqus

In this appendix, data from the mesh convergence study in Abaqus are to be found.

Table H.1 ULS-load for different mesh, uniaxial loading, Lay-up A $[0_3/+45/90/-45]_{2S}$.

	$b/t=50$		$b/t=10$	
Mesh	ULS	ULS/ULS ₂₁₁₆	ULS	ULS/ULS ₂₁₁₆
100	146.5	1.071	542.1	0.999
400	138.4	1.012	542.1	0.999
900	135.4	0.989	542.6	1.00
1024	137.0	1.001	542.6	1.00
1296	136.8	1.00	542.6	1.00
1600	136.8	1.00	542.6	1.00
2116	136.8	1.00	542.6	1.00

Table H.2 ULS-load for different mesh, uniaxial loading, Lay-up B $[-45/+45/0]_{4S}$.

	$b/t=50$		$b/t=10$	
Mesh	ULS	ULS/ULS ₂₁₁₆	ULS	ULS/ULS ₂₁₁₆
100	127.29	1.012	343.19	1.002
400	123.05	0.978	343.43	1.002
900	125.34	0.996	342.99	1.001
1024	123.56	0.982	342.70	1.00
1296	125.78	1.00	342.58	1.00
1600	125.64	0.999	342.76	1.00
2116	125.77	1.00	342.59	1.00

Table H.3 LPF for different mesh, biaxial loading, Lay-up A $[0_3/+45/90/-45]_{2S}$.

Mesh	$b/t=50$		$b/t=10$	
	LPF	LPF/LPF ₂₁₁₆	LPF	LPF/LPF ₂₁₁₆
100	80.52	1.032	257.15	1.002
400	78.19	1.003	256.67	1.00
900	78.27	1.004	256.60	1.00
1024	78.22	1.003	256.66	1.00
1296	78.13	1.002	256.63	1.00
1600	78.73	1.009	256.59	1.00
2116	77.99	1.00	256.63	1.00

Table H.4 LPF for different mesh, biaxial loading, Lay-up B $[-45/+45/0]_{4S}$.

Mesh	$b/t=50$		$b/t=10$	
	LPF	LPF/LPF ₃₂₀₀	LPF	LPF/LPF ₂₁₁₆
100	93.58	1.039	336.89	1.00
400	88.77	0.986	336.68	0.999
900	89.41	0.993	336.73	0.999
1024	89.88	0.998	336.925	1.00
1296	90.21	1.002	336.93	1.00
1600	90.65	1.006	336.97	1.00
2116	90.97	1.01	336.95	1.00
3200	90.07	1.00	-	-

Appendix I. Results

This appendix contains the results of the ULS calculations for all plates included in the study. The results are presented in Figures I.1-5 of load vs. centre out-of-plane displacement curves. Furthermore, comparisons of ULS-loads between failure criteria Hashin-Rotem and Hashin are presented in Table I.1.

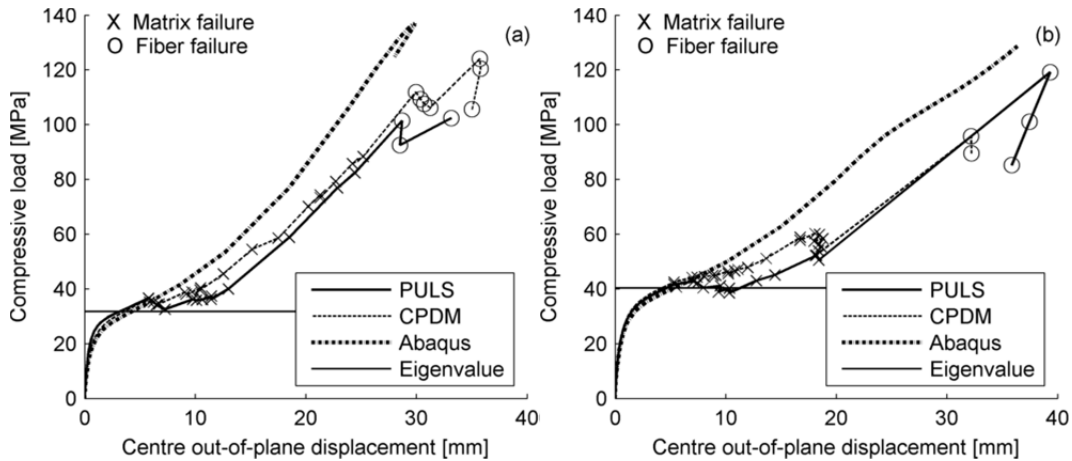


Figure I.1 Load-displacement curves for lay-up $A [0_3/+45/90/-45]_{2S}$ (a) and lay-up $B [-45/+45/0]_{4S}$ (b), both with $b/t=50$.

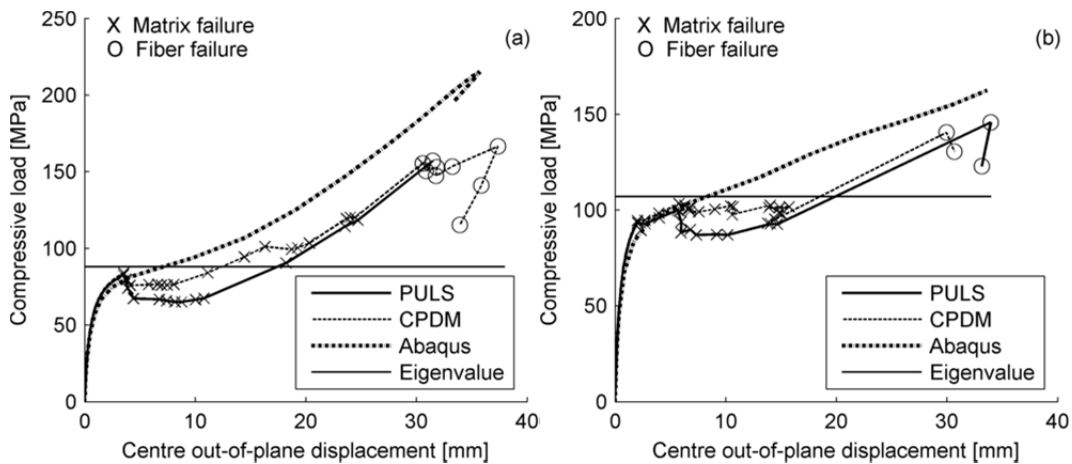


Figure I.2 Load-displacement curves for lay-up $A [0_3/+45/90/-45]_{2S}$ (a) and lay-up $B [-45/+45/0]_{4S}$ (b), both with $b/t=30$.

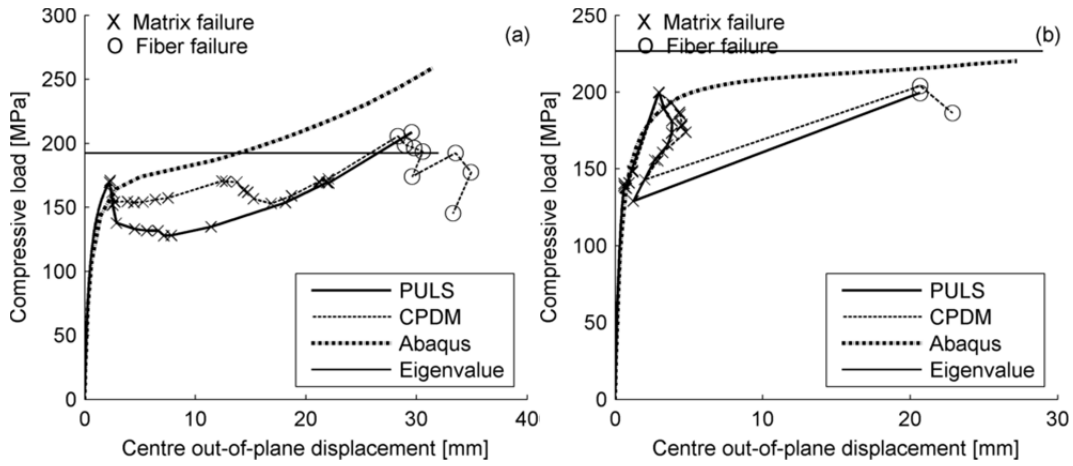


Figure I.3 Load-displacement curves for lay-up $A [0_3/+45/90/-45]_{2S}$ (a) and lay-up $B [-45/+45/0]_{4S}$ (b), both with $b/t=20$.

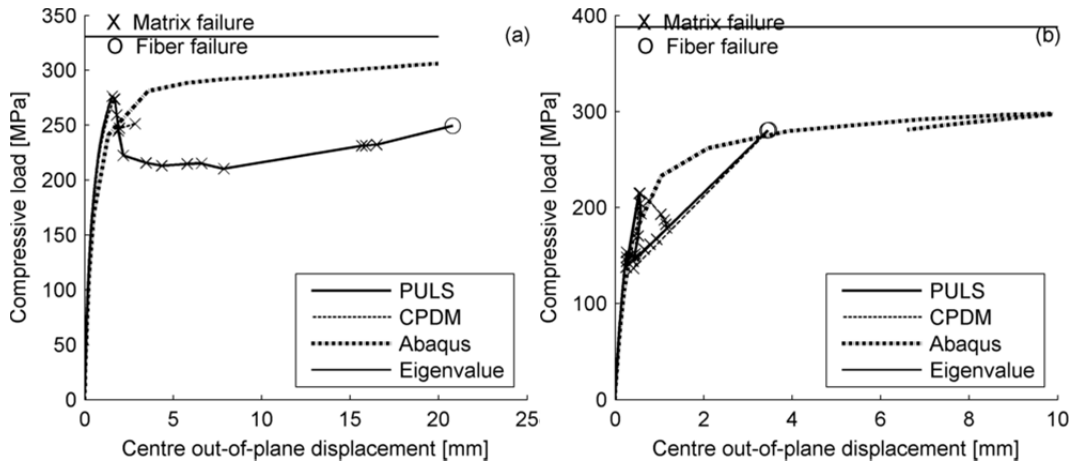


Figure I.4 Load-displacement curves for lay-up $A [0_3/+45/90/-45]_{2S}$ (a) and lay-up $B [-45/+45/0]_{4S}$ (b), both with $b/t=15$.

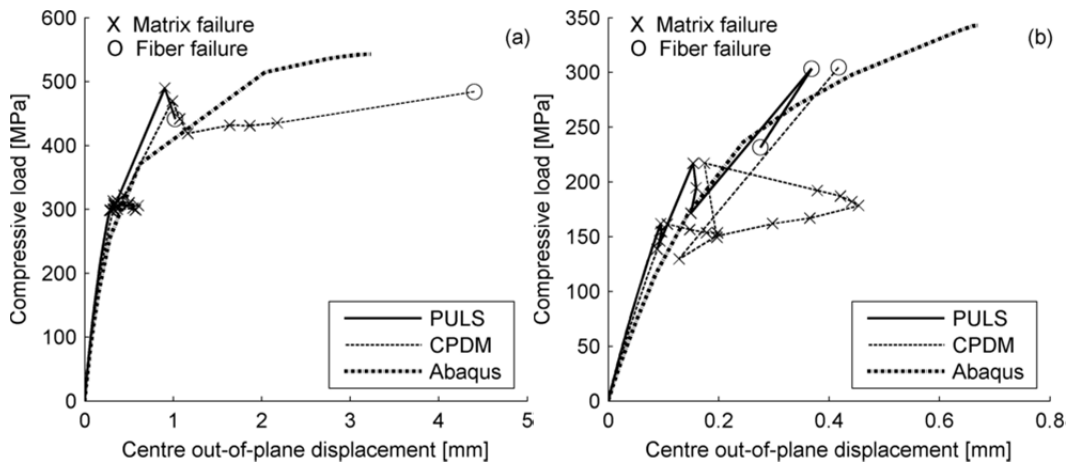


Figure I.5 Load-displacement curves for lay-up $A [0_3/+45/90/-45]_{2S}$ (a) and lay-up $B [-45/+45/0]_{4S}$ (b), both with $b/t=10$.

Table I.1 Comparison of ULS-loads between failure criteria.

ULS [MPa]			
Lay-up	b/t	Hashin-Rotem	Hashin
A	10	542.6	542.8
A	50	136.9	136.7
B	10	342.7	342.8